Elucidating modern West Antarctic sea surface conditions: An intercomparison of lipid biomarker proxies, instrumental and numerical-model data

Nele Lamping[1], Juliane Müller[1,2,3], Jens Hefter[1], Gesine Mollenhauer[1,2,3], Christian Haas[1], Xiaoxu Shi[1], Maria-Elena Vorrath[1,4], Gerrit Lohmann[1,3,5]

[1]Alfred-Wegener-Institut Helmholtz-Zentrum für Polar- und Meeresforschung, Am Alten Hafen 26, 27568 Bremerhaven, Germany

[2]Department of Geosciences, University of Bremen, Klagenfurter Straße, 28359 Bremen, Germany

[3]Marum - Center for Marine Environmental Sciences, Leobener Straße 8, 28359 Bremen, Germany

[4]Laboratoire des Sciences de l'Environnement Marin (LEMAR), Université de Bretagne Occidentale, Brest, France

[5]Department of Environmental Physics, University of Bremen, 28359 Bremen, Germany

Correspondence to: Nele Lamping (nele.lamping@awi.de)

Abstract

The importance of Southern Ocean sea ice has come into the focus of polar research in the last couple of decades. Especially in West Antarctica, where sea ice has declined, its distribution and evolution play a critical role for the stability of nearby ice shelves. Organic geochemical analyses of marine surface sediments from the West Antarctic continental shelves permit a biomarker-based reconstruction of sea surface conditions in these vulnerable areas. We analysed highly branched isoprenoids (HBIs), such as the sea-ice proxy $IPSO_{25}$ and phytoplankton-derived HBI-trienes, but also phytosterols and isoprenoidal glycerol dialkyl glycerol tetraethers (GDGTs), which are established tools for the reconstruction of primary productivity and sea surface temperatures, respectively. The combination of $IPSO_{25}$ with a

phytoplankton marker results in the semi-quantitative sea-ice index $PIPSO_{25}$, which provides useful reconstructions of sea-ice conditions, avoiding misleading over- or underestimations of sea-ice cover. Comparisons of the biomarker-based sea-ice distribution patterns and GDGT-based temperatures with (1) sea-ice distributions obtained from satellite observations and (2) estimated sea-ice patterns and SSTs deduced from modelled data are in reasonable agreement, but also highlight specific aspects that need to be considered when interpreting biomarker data. We further discuss $IPSO_{25}$ concentrations in the vicinity of ice shelves, where elevated values could be related to the occurrence of ice shelf basal melt water and platelet ice under landfast sea ice.

1. Introduction

One of the key components of the global climate system, influencing major atmospheric and oceanic processes, is floating on the ocean's surface at high latitudes – sea ice (Thomas, 2017). Southern Ocean sea ice is one of the most strongly changing features of the Earth's surface as it experiences considerable seasonal variabilities with decreasing sea-ice extent from a maximum of 20 x 10^6 km^2 in September to a minimum of 4 x 10^6 km^2 in March (Arrigo et al., 1997; Zwally, 1983). This seasonal waxing and waning of sea ice substantially modifies deep-water formation, the ocean-atmosphere exchange of heat and gas, strongly affects surface albedo and radiation budgets (Abernathey et al., 2016; Nicholls et al., 2009; Turner et al., 2017) and also regulates ocean buoyancy flux, upwelling and primary production (Schofield et al., 2018).

Southern Ocean sea-ice extent has undergone regionally contrasting changes since the beginning of satellite-based observations in 1979 (Parkinson, 2019). In the 40-year satellite record, sea-ice extent in East Antarctica is increasing, experiencing an abrupt reversal from 2014 to 2018 (~~even exceeding the drastic decay rates reported in the Arctic;~~ Comiso et al., 2017; Parkinson, 2019; Parkinson and Cavalieri, 2012). Sea-ice extent in West Antarctica, however, is decreasing since the beginning of satellite-based observations 40 years ago (Parkinson and Cavalieri, 2012). ~~Here,~~ the Antarctic Peninsula has been affected by significant changes in sea-ice duration over the past few decades, undergoing a strong decrease in sea-ice extent (Liu et al., 2004) and rapid atmospheric warming (Vaughan et al., 2003). The Larsen Ice Shelves A and B, located at the East Antarctic Peninsula, collapsed in 1995 and 2002, respectively, which ~~Massom et al. (2018)~~ linked to the loss of a sea-ice buffer, enabling an increased flexure of the ice shelf margins by ocean swells. The Bellingshausen and Amundsen Seas are also affected by a stark sea-ice decline (Hobbs et al., 2016; Parkinson, 2019). Glaciers draining into the Amundsen Sea are thinning at an alarming rate, which has been linked to basal melting caused by relatively warm Circumpolar Deep Water (CDW) incursions into sub-ice shelf cavities,

thinning the adjacent ice shelves from below (e.g., Jacobs et al., 2011). The disintegration of ice shelves reduces the buttressing force for the West Antarctic Ice Sheet, which may lead to a partial collapse of ice shelves in these catchments, eventually impacting global sea level rise significantly (Pritchard et al., 2012; Vaughan, 2008).

State-of-the-art climate models are not yet fully able to depict sea-ice seasonality and sea-ice cover, which the 5th Assessment Report of the Intergovernmental Panel on Climate Change (Stocker et al., 2013) explains by a lack of validation efforts using proxy-based sea-ice reconstructions. Knowledge about (paleo-) sea-ice conditions in the climate sensitive areas around the West Antarctic Ice Sheet is hence considered as crucial for understanding past and future climate evolution.

To date, the most common proxy-based sea-ice reconstructions in the Southern Ocean are conducted by the use of sympagic diatom assemblages, which are strongly dependent on their preservation within the sediments (Allen et al., 2011; Armand and Leventer, 2003; Crosta et al., 1998; Esper and Gersonde, 2014; Gersonde and Zielinski, 2000; Leventer, 1998). Dissolution effects within the water column or after deposition determine the preservation state of the small, lightly silicified microfossils and may alter the diatom record, leading to inaccurate sea-ice reconstructions (Leventer, 1998; Zielinski et al., 1998). To avoid ambiguous interpretations, the molecular remains of certain diatoms, specific organic geochemical lipids, have recently emerged as a robust proxy for reconstructing past (and present) Antarctic sea ice (Barbara et al., 2013; Collins et al., 2013; Denis et al., 2010; Etourneau et al., 2013; Lamping et al., 2020; Massé et al., 2011; Vorrath et al., 2019; 2020). Specifically, a di-unsaturated highly branched isoprenoid (HBI) alkene (HBI diene, $C_{25:2}$) has been detected in both sea-ice diatoms and sediments in the Southern Ocean (Johns et al., 1999; Massé et al., 2011; Nichols et al., 1988) and the sympagic (i.e. living within sea ice) tube-dwelling diatom *Berkeleya adeliensis* was recently identified as producer, which preferably proliferates in platelet ice (Belt et al., 2016; Riaux-Gobin and Poulin, 2004). However, *B. adeliensis* seems rather flexible concerning

its habitat, since it was also recorded in the bottom ice layer and seems to be well adapted to changes in texture during ice melt (Riaux-Gobin et al., 2013). Belt et al. (2016) introduced the term $IPSO_{25}$ ("Ice Proxy of the Southern Ocean with 25 carbon atoms") because of the structurally close relationship of this lipid to the counterpart IP_{25} in the Arctic. Hitherto, only a relatively small number of studies based on $IPSO_{25}$ for recent and Holocene sea-ice reconstructions is available in the Southern Ocean (Barbara et al., 2010; 2013; Belt et al., 2016; 2018; Collins et al., 2013; Denis et al., 2010; Etourneau et al., 2013; Lamping et al., 2020; Massé et al., 2011; Tesi et al., 2020; Vorrath et al., 2019; 2020). Commonly, for a more detailed assessment of sea-ice conditions, IP_{25} in the Arctic Ocean and $IPSO_{25}$ in the Southern Ocean have been measured alongside complementary phytoplankton derived lipids, such as sterols and/or HBI-trienes, which are indicative of open-water conditions (Belt and Müller, 2013; Lamping et al., 2020; Müller et al., 2011; Vorrath et al., 2019; 2020). The combination of the sea-ice biomarker and a phytoplankton biomarker, the so called PIP_{25} index for the Arctic (Müller et al., 2011) and the $PIPSO_{25}$ index for the Antarctic (Vorrath et al., 2019), allow for a more quantitative differentiation of contrasting sea-ice settings. A misinterpretation of an absent sea-ice biomarker, which can be the result of either no sea-ice cover or a severe sea-ice cover, that prevents light penetration hence limiting ice algae growth, can be circumvented with this approach.

Mechanisms contributing to ice shelf instability are manifold. As previously mentioned, relatively warm CDW is considered one of the main drivers for ice shelf thinning in the Amundsen Sea Embayment (Jacobs et al., 2011; Jenkins and Jacobs, 2008). Accordingly, changing ocean temperatures are another crucial factor for the fate of West Antarctic Ice Sheet stability (e.g., Colleoni et al., 2018). As for sea-ice reconstructions, organic geochemical lipids for reconstructing past and recent ocean temperatures in high latitudes have come into focus in the past decades, since the preservation of calcium carbonate microfossils is not continuous in high latitude sediments (e.g., Zamelczyk et al., 2012). Archaeal isoprenoidal glycerol dialkyl

79 glycerol tetraethers (isoGDGTs), sensitive to temperature change and relatively resistant to
80 degradation processes, are well-preserved in marine sediments (Huguet et al., 2008; Schouten
81 et al., 2013). Hence, isoGDGTs are considered to be valuable tools for reconstructing ocean
82 temperatures (Schouten et al., 2002).

83 Our aim with this study is to provide insight into the application of biomarkers for sea ice as
84 well as ocean temperature reconstructions. Estimates on recent sea-ice conditions along the
85 eastern and western Antarctic Peninsula, the Amundsen and Weddell Seas, are based on the
86 analyses of $IPSO_{25}$, HBI-trienes and phytosterols in surface sediment samples from these areas.
87 We further address the potential connection between $IPSO_{25}$ and platelet ice formation under
88 near-coastal fast ice, which is related to the presence of near-surface ice shelf basal melt water.
89 An intercomparison of sea ice as well as temperature reconstructions (based on GDGT
90 analyses) with (1) sea-ice distributions obtained from satellite observations and (2) estimated
91 sea-ice distribution and SSTs deduced from modelled data provides for an evaluation of the
92 proxy approaches. For a more semi-quantitative sea-ice estimate, the relatively new approach
93 of $PIPSO_{25}$ has been used to further assess the advantages and limitations of the sea-ice index
94 as a potential tool to validate and improve numerical climate models to better understand
95 current and past trends in sea-ice development in the Southern Ocean.

2. Regional setting

The areas of investigation in this study include the southern Drake Passage, the continental shelves of the West and East Antarctic Peninsula (~ 60° S) and the more southerly located Amundsen and Weddell Seas (~ 75° S; Fig. 1). The different study areas are all connected by the only current circumnavigating the globe, the Antarctic Circumpolar Current (ACC; Meredith et al., 2011; Rintoul et al., 2001).

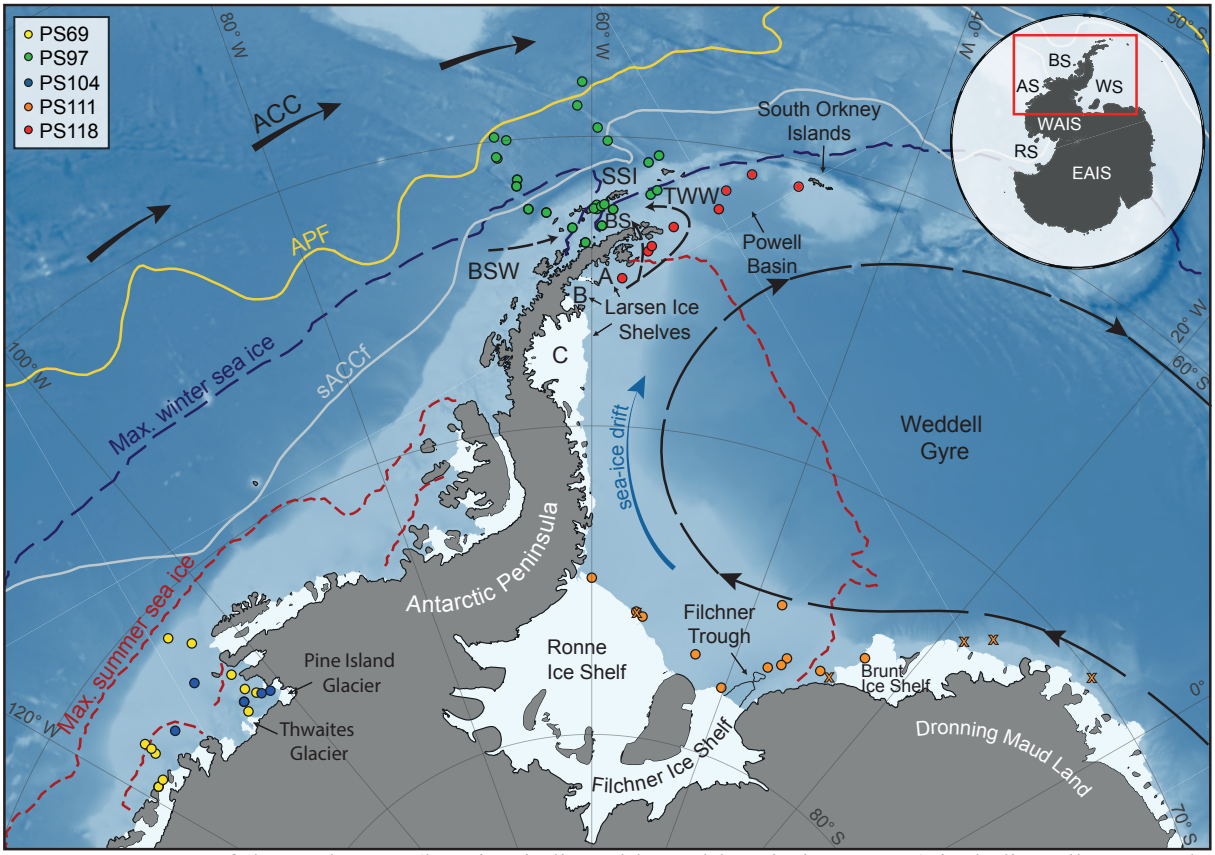

Fig. 1: Map of the study area (location indicated by red box in insert map) including all 41 sample locations (see different colored dots for individual FS Polarstern expeditions in the top left corner; for detailed sample information see Table S1) and main oceanographic features. Max. summer and winter sea-ice boundaries are marked by dashed red and blue line, respectively (Fetterer et al., 2016). Orange crosses indicate samples where a $PIPSO_{25}$ value of 1 has been assigned due to low biomarker concentrations, close to detection limit. ACC: Antarctic Circumpolar Current, APF: Antarctic Polar Front, sACCf: southern Antarctic Circumpolar Current Front, SSI: South Shetland Islands, BS: Bransfield Strait, BSW: Bellingshausen Sea Water, TWW: Transitional Weddell Sea Water (Mathiot et al., 2011; Orsi et al., 1995). Insert map shows grounded ice only (i.e., no ice shelves), WAIS: West Antarctic Ice Sheet, EAIS: East Antarctic Ice Sheet, RS: Ross Sea, AS: Amundsen Sea, BS: Bellingshausen Sea, WS: Weddell Sea. Background bathymetry derived from IBCSO data (Arndt et al., 2013).

The ACC is the largest current system in the world characterised by a strong eastward flow, which finds its narrowest constriction in the Drake Passage. It is mainly composed of CDW, which is generally divided into the Upper CDW with low oxygen and high nutrient

concentrations, and Lower CDW with high salinities (Rintoul et al., 2001). Along the Bellingshausen Sea, the Amundsen Sea and West Antarctic Peninsula (i.e., the Bransfield Strait), where the ACC flows close to the continental shelf edge, CDW is upwelling onto the shelf via bathymetric troughs, contributing to basal melt and retreat of the adjoining ice shelves (Jacobs et al., 2011; Jenkins and Jacobs, 2008; Klinck et al., 2004). In the Weddell Sea, where the ACC is located sufficiently far from the Antarctic continent, a subpolar cyclonic circulation is present south of the ACC, the Weddell Gyre. The Weddell Gyre is the main circulation in the Weddell Sea and the most important source of Antarctic Bottom Water (Deacon, 1979), with sea-ice formation as an important factor in generating these dense water masses (Harms et al., 2001). Wind and currents force a northward sea-ice drift in the western Weddell Sea along the coast of the East Antarctic Peninsula (Harms et al., 2001) until leaving it to melt in warmer waters to the North and up to the Powell Basin (Vernet et al., 2019). At the northern tip of the Antarctic Peninsula, Transitional Weddell Sea Water (TWW) branches off into the Bransfield Strait and is characterised by colder temperatures and higher salinities as a result of extended sea-ice formation in the Weddell Gyre (Collares et al., 2018; Thompson et al., 2009). Here, it encounters the well-stratified, warm, and fresh Bellingshausen Sea Water (BSW; Fig. 1), which is entering the Bransfield Strait from the West (Sangrà et al., 2011).

Since 1978, satellite observations show strong seasonal shifts of sea-ice cover at the Antarctic Peninsula, which is less pronounced in the more southerly Amundsen and Weddell Seas (Fig. 2a-c). Mean monthly sea-ice concentrations (SIC) for winter (JJA), spring (SON) and summer (DJF) reveal a permanently ice-free Drake Passage, while the West and East Antarctic Peninsula shelf areas are influenced by a changing sea-ice cover in the course of a year (Fig. 2a-c). For the Amundsen and Weddell Seas, satellite data reveal a closed seasonal

128 sea-ice cover with up to ~ 90 % concentration during winter and spring (Fig. 2a+b), and a late

129 break-up of sea-ice cover to a minimum concentration of ~ 30 % during summer (Fig. 2c).

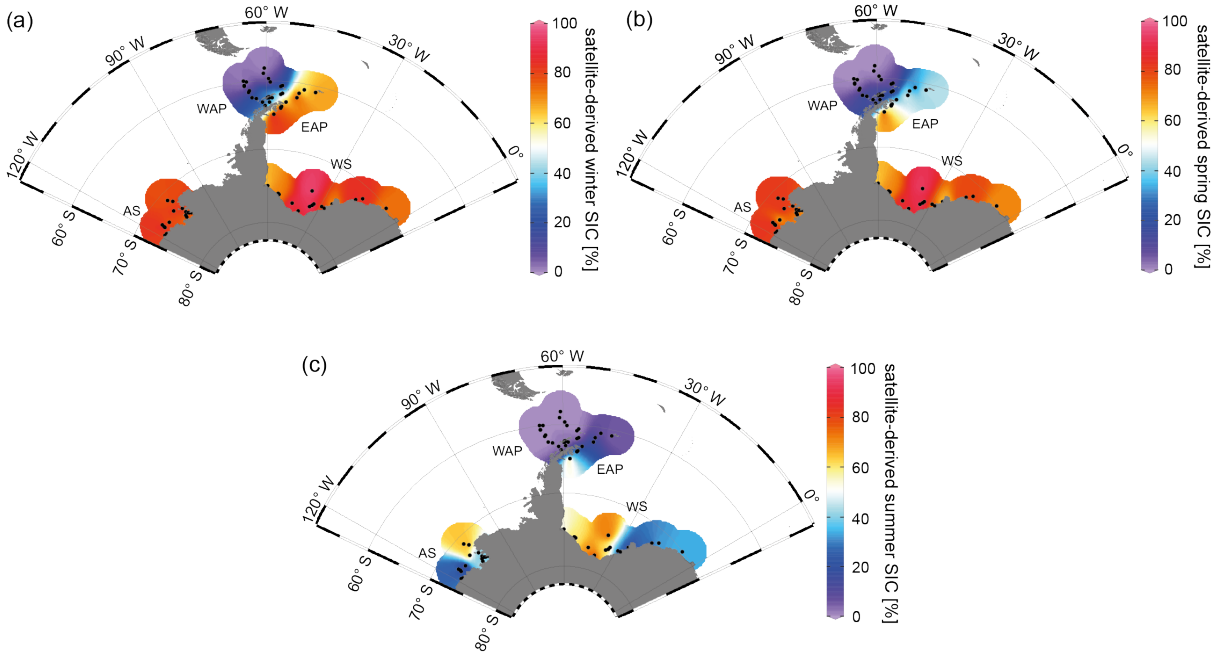

Fig. 2: Distribution of mean monthly satellite-derived sea-ice concentrations for (a) winter (JJA), (b) spring (SON) and (c) summer (DJF) in % (downloaded from the National Snow and Ice Data Center, NSIDC; Cavalieri et al., 1996). AS: Amundsen Sea, WAP: West Antarctic Peninsula, EAP: East Antarctic Peninsula, WS: Weddell Sea.

3. Material and methods

3.1 Sediment material

In total, we analysed a set of 41 surface sediment samples from different areas of the Southern Ocean (Fig. 1), all have been retrieved by multicorers during *RV Polarstern* expeditions in the past years. ~~16~~ surface sediment samples from the Amundsen Sea continental shelf were collected during *RV Polarstern* expeditions PS69 in 2007 (Gohl, 2007) and PS104 in 2017 (Gohl, 2017). ~~25~~ surface sediment samples from the southeastern and southwestern Weddell Sea continental shelf were collected during *RV Polarstern* expeditions PS111 in 2018 (Schröder, 2018) and PS118 in 2019 (Dorschel, 2019). This set of samples was complemented by 26 surface sediment samples from the Bransfield Strait/West Antarctic Peninsula for which the analytical results were already published by Vorrath et al. (2019).

3.2 Bulk sediment and organic geochemical analyses

The sediment material was freeze-dried and homogenized with an agate mortar and stored in glass vials at -20 °C before and after these initial preparation steps to avoid degradation of targeted molecular components. The analysis of total organic carbon (TOC) contents was conducted on 0.1 g of sediment after removing inorganic carbon (total inorganic carbon, carbonates) with 500 µl 12 N hydrochloric acid. Measurements were conducted by means of a carbon-sulphur determinator (CS 2000; Eltra) with standards being measured for calibration before sample analyses and after every tenth sample to ensure accuracy (error ± 0.02 %).

Lipid biomarker extraction of the sediment (4 g for PS69 and PS104; 6 g for PS111 and PS118) was done by ultrasonication (3 x 15 min), using dichloromethane:methanol (3 x 6 ml for PS69 and PS104; 3 x 8 ml for PS111 and PS118; 2:1 v/v) as solvent. Prior to this step, the internal standards 7-hexylnonadecane (7-HND; 20 µl/sample for PS69 and PS104 and 30 µl/sample for PS111 and PS118), 5α-androstan-3-ol (40 µl/sample) and C_{46} (100 µl/sample) were added to the sample for quantification of HBIs, sterols and GDGTs, respectively. Via

156 open-column chromatography, with SiO_2 as stationary phase, fractionation of the extract was
157 achieved by eluting the apolar fraction (HBIs) and the polar fraction (sterols and GDGTs) with
158 5 ml n-hexane and 5 ml DCM/MeOH 1:1, respectively. The polar fraction was subsequently
159 split into two fractions (sterols and GDGTs) for further processing. The sterol fraction was
160 silylated with 300 µl bis-trimethylsilyl-trifluoroacetamide (BSTFA; 2h at 60 °C). Compound
161 analyses of HBIs and sterols were carried out on an Agilent Technologies 7890B gas
162 chromatograph (GC; fitted with a 30 m DB 1MS column; 0.25 mm diameter and 0.25 µm film
163 thickness) coupled to an Agilent Technologies 5977B mass selective detector (MSD; with 70
164 eV constant ionization potential, ion source temperature of 230 °C). The GC oven was set to:
165 60 °C (3 min), 150 °C (rate: 15 °C/min), 320 °C (rate: 10 °C/min), 320 °C (15 min isothermal)
166 for the analysis of hydrocarbons and to: 60 °C (2 min), 150 °C (rate: 15 °C/min), 320 °C (rate:
167 3 °C/min), 320 °C (20 min isothermal) for the analysis of sterols. Helium was used as carrier
168 gas. The identification of HBI and sterol compounds is based upon their GC retention times
169 and mass spectra (Belt, 2018; Belt et al., 2000; Boon et al., 1979). Lipid quantification was
170 obtained by setting the individual, manually integrated, GC-MS peak area in relation to the
171 peak area of the respective internal standard and normalization to the amount of extracted
172 sediment. Quantification of $IPSO_{25}$ and HBI Z-triene was achieved using their molecular ion
173 ($IPSO_{25}$: m/z 348 and HBI Z-triene: m/z 346) in relation to the fragment ion m/z 266 of the
174 internal standard 7-HND (Belt, 2018). Quantification of sterols was achieved by comparison of
175 the fragment ion of the individual sterol with the fragment ion m/z 348 of the internal standard
176 5α-androstan-3-ol. Instrumental response factors for the target lipids were considered as
177 recommended by Belt et al. (2014) and Fahl and Stein (2012). All biomarker concentrations
178 were subsequently normalized to the TOC content of each sample to account for different
179 depositional settings within the different study areas.

180 For calculating the phytoplankton-$IPSO_{25}$ ($PIPSO_{25}$) index, we used the equation introduced
181 by Vorrath et al. (2019):

$$PIPSO_{25} = IPSO_{25} / (IPSO_{25} + (phytoplankton\ marker\ x\ c)) \quad (1)$$

where c (c = mean $IPSO_{25}$/mean phytoplankton marker) is applied as a concentration balance factor to account for high concentration offsets between $IPSO_{25}$ and the phytoplankton biomarker (see Table S1 for c-factors of individual $PIPSO_{25}$ calculations).

Following the approach by Müller and Stein (2014) and Lamping et al. (2020), samples with exceptionally low (at detection limit) concentrations of both biomarkers have been assigned a $PIPSO_{25}$ value of 1 (see chapter 4.1.2). This accounts for five sample stations in the Weddell Sea PS111/13-2, /15-1, /16-3, /29-3; /40-2 (marked as orange x in Fig. 1).

The GDGT fraction was dried under N_2, redissolved with 120 µl hexane:isopropanol (v/v 99:1) and then filtered using a polytetrafluoroethylene (PTFE) filter with a 0.45 µm pore sized membrane. GDGT measurements were carried out using high performance liquid chromatography (HPLC; Agilent 1200 series HPLC system) coupled to an Agilent 6120 mass spectrometer (MS), operating with atmospheric pressure chemical ionization (APCI). The injection volume was 20 µl. For separating the GDGTs, a Prevail Cyano 3 µm column (Grace, 150 mm * 2.1 mm) was kept at 30 °C. Each sample was eluted isocratically for 5 min with solvent A = hexane/2-propanol/chloroform; 98:1:1 at a flow rate of 0.2 ml/min, then the volume of solvent B = hexane/2-propanol/chloroform; 89:10:1 was increased linearly to 10 % within 20 min and then to 100 % within 10 min. The column was back-flushed (5 min, flow 0.6 ml/min) after 7 min after each sample and re-equilibrated with solvent A (10 min, flow 0.2 ml/min). The APCI was set to the following: N_2 drying gas flow at 5 l/min and temperature to 350 °C, nebulizer pressure to 50 psi, vaporizer gas temperature to 350 °C, capillary voltage to 4 kV and corona current to +5 µA. Detection of GDGTs was achieved by means of selective ion monitoring (SIM) of $[M+H]^+$ ions (dwell time 76 ms). Determination and quantification of the molecular ions of GDGT-0 (*m/z* 1302), GDGT-1 (*m/z* 1300), GDGT-2 (*m/z* 1298), GDGT-3 (*m/z* 1296) and crenarchaeol (*m/z* 1292) as well as of brGDGT-III (*m/z* 1050), brGDGT-II (*m/z* 1036) and brGDGT-I (*m/z* 1022) was done in relation to the molecular ion *m/z* 744 of the

internal standard C_{46}-GDGT. The late eluting hydroxylated GDGTs (OH-GDGT-0, OH-GDGT-1 and OH-GDGT-2 with *m/z* 1318, 1316 and 1314, respectively) were quantified in the scans (*m/z* 1300, 1298, 1296) of their related GDGTs, as described by Fietz et al. (2013).

TEX^{L}_{86} values and their conversion into temperatures were determined following Kim et al. (2010):

$$TEX^{L}_{86} = \mathrm{LOG}\frac{[GDGT-2]}{[GDGT-1]+[GDGT-2]+[GDGT-2]}, \quad (2)$$

$$SST^{TEX}\ [°C] = 67.5\,x\,TEX^{L}_{86} + 46.9. \quad (3)$$

Temperature calculations based on OH-GDGTs were carried out according to Lü et al. (2015):

$$RI-OH' = \frac{[OH-GDGT-1]+2\,x\,[OH-GDGT-2]}{[OH-GDGT-0]+[OH-GDGT-1]+[OH-GDGT-2]}, \quad (4)$$

$$SST^{OH}\ [°C] = (RI-OH' - 0.1) / 0.0382. \quad (5)$$

To determine the relative influence of terrestrial organic matter input, the BIT-index was calculated following Hopmans et al. (2004):

$$BIT = \frac{[brGDGT-I]+[brGDGT-II]+[brGDGT-III]}{[Chrenarchaeol]+[brGDGT-I]+[brGDGT-II]+[brGDGT-III]}. \quad (6)$$

3.3 Numerical model

3.3.1 Model description

AWI-ESM2 is a state-of-the-art coupled climate model developed by Sidorenko et al. (2019) which comprises an atmospheric component ECHAM6 (Stevens et al., 2013) as well as an ocean-sea ice component FESOM2 (Danilov et al., 2017). The atmospheric module ECHAM6 is the most recent version of the ECHAM model developed at the Max Planck Institute for Meteorology (MPI) in Hamburg. The model is branched from an early release of the European Center (EC) for Medium Range Weather Forecasts (ECMWF) model (Roeckner et al., 1989). ECHAM6 dynamics is based on hydrostatic primitive equations with traditional approximation. We used T63 Gaussian grid which has a spatial resolution of about 1.9 x 1.9 degree (1.9 ° or 210 km). There are 47 vertical layers in the atmosphere.

Momentum transport arising from boundary effects is configured using the subgrid orography scheme as described by Lott (1999). Radiative transfer in ECHAM6 is represented by the method described in Iacono et al. (2008). ECHAM6 also contains a Land-Surface Model (JSBACH) which includes 12 functional plant types of dynamic vegetation and 2 bare-surface types (Loveland et al., 2000; Raddatz et al., 2007). The ice-ocean module in AWI-ESM2 is based on the finite volume discretization formulated on unstructured meshes. The multi-resolution for the ocean is up to 15 km over polar and coastal regions, and 135 km for far-field oceans, with 46 uneven vertical depths. The impact of local dynamics on the global ocean is related to a number of FESOM-based studies (Danilov et al., 2017). The multi-resolution approach advocated by FESOM allows one to explore the impact of local processes on the global ocean with moderate computational effort (Danilov et al., 2017). AWI-ESM2 employs the OASIS3-MCT coupler (Valcke, 2013) with an intermediate regular exchange grid. Mapping between the intermediate grid and the atmospheric/oceanic grid is handled with bilinear interpolation. The atmosphere component computes 12 air–sea fluxes based on four surface fields provided by the ocean module FESOM2. AWI-ESM2 has been validated under modern climate conditions (Sidorenko et al., 2019) and has been applied for marine radiocarbon concentrations (Lohmann et al., 2020), the latest Holocene (Vorrath et al., 2020), and the Last Interglacial (Otto-Bliesner et al., 2021).

3.3.2 Experimental design

One transient experiment was conducted using AWI-ESM2, which applied the boundary conditions, including orbital parameters and greenhouse gases. Orbital parameters are calculated according to Berger (1978), and the concentrations of greenhouse gases are taken from ice-core records as well as from recent measurements of firn air and atmospheric samples (Köhler et al., 2017). The model was initialized from a 1,000-year spin-up run under mid-Holocene boundary conditions as described (Otto-Bliesner et al., 2017). In our modeling

strategy, we follow Lorenz and Lohmann (2004) and use the climate condition from the preindustrial state as spin-up and initial state for the subsequent transient simulation covering the period 1950-2014 CE. Topography including prescribed ice sheet was kept constant in our transient simulation. All model data are provided in Table S2.

3.4. Satellite SIC and SSTs

Satellite data are derived from Nimbus-7 SMMR and DMSP SSM/I-SSMIS passive microwave data and downloaded from the National Snow and Ice Data Center (NSIDC; Cavalieri et al., 1996). The sea-ice data represent mean monthly SIC, which are expressed to range from 0 % to 100 % and are averaged over a period of the beginning of satellite observations in 1978 to the individual year of sample retrieval. The monthly mean SIC were then split into different seasons: winter (JJF), spring (SON) and summer (DJF) (Fig. 2a-c) and the data are considered to represent the recent mean state of sea-ice coverage. All satellite data are provided in Table S3.

Modern annual mean SSTs are derived from the World Ocean Atlas 13 representing averaged values for the years 1955-2012 (Fig. 5c; WOA13; Locarnini et al., 2013).

4. Results and discussion

4.1 Environmental settings of the Southern Ocean depicted by proxy data

In the following, we describe the biomarker and model data assembled during this study from North (Antarctic Peninsula) to South (Amundsen and Weddell Seas) and draw conclusions about the environmental settings deduced from the data set. All biomarker data collected during this study are provided in Table S1 and are available via the PANGAEA data repository (in prep.).

4.1.1 TOC content, HBIs and sterols in Antarctic surface sediments

TOC contents in marine sediments in a first approximation are often viewed as an indicator for primary productivity in surface waters (Meyers, 1997), ~~however~~ we are aware that additional factors, such as different water depths or depositional regimes, may exert control on sedimentary TOC as well. The TOC contents of the herein investigated surface samples are lowest in the Drake Passage with values around 0.12-0.54 %, increasing in a northwest-southeast gradient into the Bransfield Strait, ranging between 0.59-1.06 % (Fig. 3a; WAP).

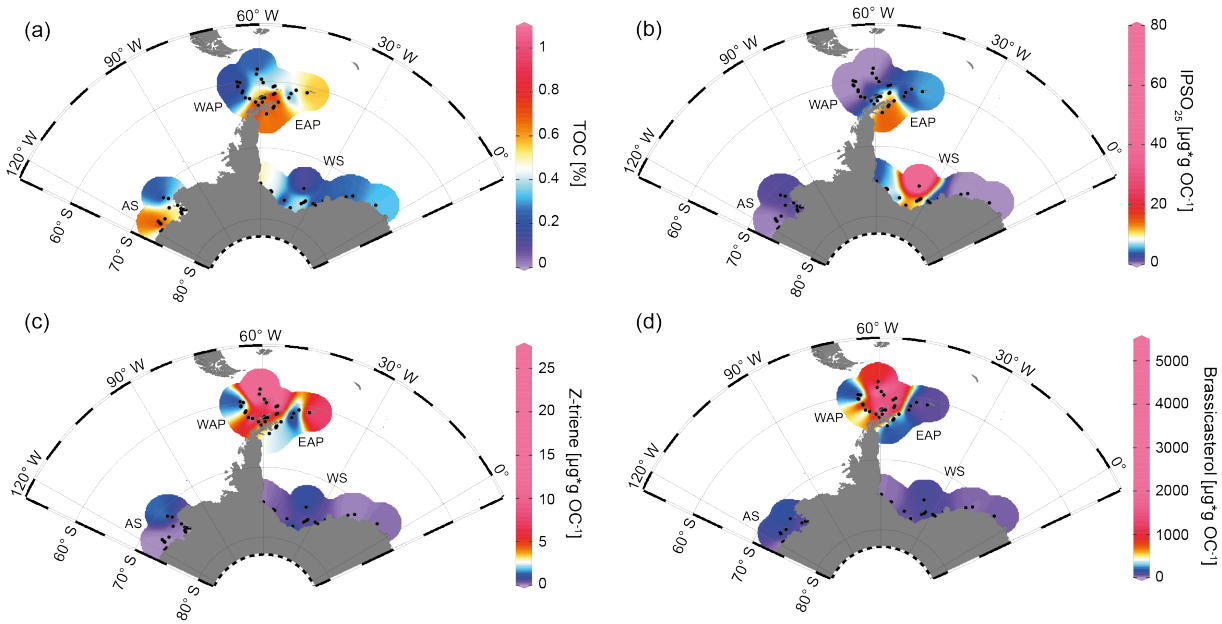

Fig. 3: Distribution of (a) TOC [%], (b) $IPSO_{25}$, (c) Z-triene and (d) brassicasterol in surface sediment samples. Sample locations are marked as black dots. Concentrations of biomarkers [µg*g OC^{-1}] were normalized to the TOC content of each sample. AS: Amundsen Sea, WAP: West Antarctic Peninsula, EAP: East Antarctic Peninsula, WS: Weddell Sea.

290 At the East Antarctic Peninsula, higher TOC contents (0.57-0.86 %) prevail around the
291 Larsen Ice Shelf with a decreasing trend towards the Powell Basin (0.22-0.37 %) and an
292 increase to 0.50 % around the area of the South Orkney Islands, pointing to elevated
293 productivity in these areas (Fig. 3a; EAP). The elevated TOC contents in this area may,
294 however, also be attributable to higher inputs of reworked terrigenous organic matter.
295 At the West Antarctic Peninsula, concentrations of the sea-ice biomarker $IPSO_{25}$ show a
296 northwest-southeast gradient with $IPSO_{25}$ being absent in samples from the permanently ice-
297 free Drake Passage and increasing concentrations towards the continental slope and the
298 seasonally ice-covered continental shelf (0.37-17.81 μg*g OC^{-1}; Fig. 3b; Vorrath et al., 2019).
299 Highest $IPSO_{25}$ concentrations are observed in samples of the northern Bransfield Strait
300 affected by TWW inflow through the Antarctic Sound and along the Antarctic Peninsula which
301 frequently exports sea ice from the Weddell Sea into the Bransfield Strait (Vorrath et al., 2019).
302 High $IPSO_{25}$ concentrations are also observed at the East Antarctic Peninsula, influenced by a
303 seasonal sea-ice cover, where relatively higher concentrations of the sea-ice biomarker prevail
304 in those samples located in front of the Larsen Ice Shelf (12.59-17.74 μg*g OC^{-1}; Fig. 3b). As
305 these locations are also influenced by the northward drift of sea ice by the Weddell Gyre (Fig.
306 1), the elevated $IPSO_{25}$ concentrations could also result from sea ice advected from the southern
307 Weddell Sea. We suggest that the decreasing $IPSO_{25}$ concentrations towards the Powell Basin
308 and the South Orkney Islands (0.59-5.36 μg*g OC^{-1}; Fig. 3b) can be connected to the warmer
309 ocean temperatures towards the North and increased sea-ice melt during spring and summer.
310 Concentrations of the phytoplankton biomarker HBI Z-triene around the Antarctic Peninsula
311 are highest in the eastern Drake Passage and along the continental slope (where $IPSO_{25}$ is
312 absent) and with lower concentrations in the Bransfield Strait (0.33-26.86 μg*g OC^{-1}; Fig. 3c;
313 Vorrath et al., 2019). Elevated HBI Z-triene concentrations have thus far been detected in
314 surface waters along an ice edge (Smik et al., 2016) and hence suggested to be a proxy for MIZ
315 conditions (Belt et al., 2015; Collins et al., 2013; Schmidt et al., 2018). Vorrath et al. (2019),

however, relate the high concentrations of HBI Z-triene at the northernmost stations in the permanently ice-free eastern Drake Passage to their proximity to the Antarctic Polar Front. Here, productivity of the source diatoms of HBI-trienes may be enhanced by meander-induced upwelling leading to increased nutrient flux to surface waters (Moore and Abbott, 2002). Moderate concentrations along the continental slope of the West Antarctic Peninsula and in the Bransfield Strait have been associated with elevated inflow of warm BSW which lead to a retreating sea-ice margin during spring and summer (for more details, see Vorrath et al. (2019) and Vorrath et al. (2020). Samples from the East Antarctic Peninsula continental shelf and the Powell Basin are characterised by relatively low concentrations of HBI Z-triene (Fig. 3c; ~~where $IPSO_{25}$ concentrations are highest;~~ 0.1-2.37 µg*g OC^{-1}~~; Fig. 3b),~~ showing a southwest-northeast gradient, while the northernmost sample closest to the South Orkney Islands is characterized by higher HBI Z-triene concentration of ~ 8.49 µg*g OC^{-1} (Fig. 3c; EAP). This relatively high concentration may be related to an "Island Mass Effect", coined by Doty and Oguri (1956), which refers to an increased primary production around oceanic islands in comparison to surrounding waters. Nolting et al. (1991) found extraordinarily high dissolved iron levels (as high as 50-60 nM) on the shelf of the South Orkney Islands and Nielsdóttir et al. (2012) also observed enhanced iron and Chl *a* concentrations in the vicinity of the South Orkney Islands. They connect, among others, the increased iron levels with input from seasonally retreating sea ice, which is recorded by satellites (Fig. 2a-c) and leads to a substantial annual phytoplankton bloom, which may also cause the elevated TOC contents in that sample (Fig. 3a). We assume that these conditions are favourable for the growth of the source diatoms of HBI Z-triene, leading to elevated concentrations. In the Drake Passage and the East Antarctic Peninsula, brassicasterol displays a similar pattern as the HBI Z-triene, with relatively higher concentrations (more than 2 magnitudes) ranging between 1.86 and 5017.44 µg*g OC^{-1} (Fig. 3d). In the sample closest to the South Orkney Islands, however, brassicasterol concentrations

are not elevated, unlike the HBI Z-triene (Fig. 3d; EAP), which could refer to different environmental preferences of the source organisms producing the individual biomarkers.

In the Weddell Sea, TOC contents are generally lower (< 0.4 %), with slightly elevated values in the West (up to 0.50 %) and right in front of the Filchner Ice Shelf (up to 0.52 %) (Fig. 3a). The Amundsen Sea is characterized by slightly higher TOC contents, with concentrations of up to 0.91 % in the West and lower values in the East (0.33 %; Fig. 3a; AS).

In the samples from the Amundsen and Weddell Seas, dominated by a strong winter sea-ice cover lasting until spring (Fig. 2a-c), all three biomarkers ~~are~~ low concentrate~~d~~. An exception can be observed in samples ~~from right~~ in front of the Filchner Ice Shelf with significantly higher concentrations of $IPSO_{25}$ (7.09-73.87 µg*g OC^{-1}; Fig. 3b; WS). Concentrations of $IPSO_{25}$ on the Amundsen Sea shelf are relatively low (0.04-3.3 µg*g OC^{-1}) with slightly higher values towards the north-east (Fig. 3b; AS). HBI Z-triene ~~is~~ also very low concentrate~~d~~, showing slightly higher concentrations within the Filchner Trough (0.04-1 µg*g OC^{-1}) and towards the more distal locations in the northeast of the Amundsen Sea (0.01-1.88 µg*g OC^{-1}; Fig. 3c). Brassicasterol generally shows similar patterns as the HBI Z-triene, with concentrations ranging between 1.86 and 220.54 µg*g OC^{-1} (Fig. 3d; for HBI E-triene and dinosterol distribution, see Fig. S1).

4.1.2 Combining individual biomarker records: the $PIPSO_{25}$ index

Targeting at a more quantitative assessment of sea-ice conditions, Vorrath et al. (2019) have followed the PIP_{25} index applied in the Arctic (Belt and Müller, 2013; Müller et al., 2011; Xiao et al., 2015) and introduced an equivalent sea-ice index for the Southern Ocean: $PIPSO_{25}$. The $PIPSO_{25}$ index combines the relative concentrations of the sea-ice biomarker $IPSO_{25}$ with a selected phytoplankton biomarker (P), such as HBI-trienes and sterols, as indicator for an open-ocean environment (Vorrath et al., 2019). The combination of both end members (sea ice vs. open-ocean) prevents misleading interpretations regarding the absence of $IPSO_{25}$ in the

sediments, which can be the result of two entirely different scenarios. At heavy/perennial sea-ice conditions, the thickness of sea ice hinders light penetration, thereby limiting the productivity of bottom sea-ice algae (Hancke et al., 2018). This scenario may result in the absence of both phytoplankton and sea-ice biomarkers in the sediment. The other scenario is dominated by a permanently open ocean, where the sea-ice biomarker is absent as well, but here, the phytoplankton biomarkers are present in variable concentrations (Müller et al., 2011). The presence of both biomarkers in the sediment is indicative of seasonal sea-ice coverage and/or the occurrence of stable ice margin conditions, promoting biosynthesis of both biomarkers (Müller et al., 2011). We here distinguish between P_ZIPSO_{25} and P_BIPSO_{25} using HBI Z-triene and brassicasterol as phytoplankton biomarker, respectively (Fig. 4; for $PIPSO_{25}$ values based on HBI E-triene and dinosterol see Table S1 and Fig. S2).

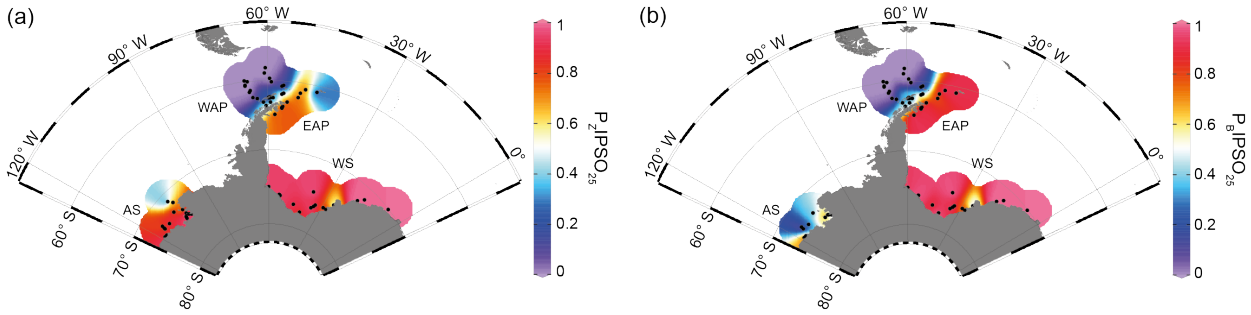

Fig. 4: Distribution of the sea-ice index $PIPSO_{25}$ in surface sediment samples, with (a) P_ZIPSO_{25} based on Z-triene and (b) P_BIPSO_{25} based on brassicasterol. AS: Amundsen Sea, WAP: West Antarctic Peninsula, EAP: East Antarctic Peninsula, WS: Weddell Sea.

Both $PIPSO_{25}$ indices are 0 in the predominantly ice-free Drake Passage and display a northwest-southeast gradient to intermediate values towards the continental slope and the South Shetland Islands, reflecting increased influence of marginal sea-ice cover towards the coast (0.02-0.70; Vorrath et al., 2019). At the seasonally sea-ice influenced East Antarctic Peninsula, P_ZIPSO_{25} values reach 0.84, while lower values of around 0.25 are observed close to the South Orkney Islands, which relates to the elevated HBI Z-triene concentrations at that station (Fig. 3c; EAP). The P_BIPSO_{25} index, however, reveals even higher values at the East Antarctic Peninsula/northwestern Weddell Sea of up to 0.98 with no elevated values towards the South

Orkney Islands. These elevated $PIPSO_{25}$ indices align well with the significant northward ice-drift in that region by the Weddell Gyre, which leads to high proximal sea-ice coverage at the East Antarctic Peninsula.

In samples from the southern Weddell Sea, both $PIPSO_{25}$ indices show a similar pattern with high values up to 0.9, and slightly lower values in front of the Brunt Ice Shelf (0.6; Fig. 4). Very low concentrations (close to detection limit) of both biomarkers in samples located on the continental shelf off Dronning Maud Land (Fig. 1) result in low $PIPSO_{25}$ values, strongly underestimating the sea-ice cover in that area. Regarding the satellite-derived sea-ice data, this area of the continental shelf is influenced by a severe seasonal sea-ice cover. As previously mentioned, we followed the approach by Müller and Stein (2014) and Lamping et al. (2020) and assigned a maximum $PIPSO_{25}$ value of 1 to these samples to circumvent misleading interpretations and aid visualisation.

Interestingly, we obtained an intermediate $PIPSO_{25}$ value (~ 0.51) derived for one sample in front of the Brunt Ice Shelf, which may be indicative of a less severe sea-ice cover in that area. A possible explanation for the relatively lower $PIPSO_{25}$ value may be the presence of a coastal polynya that has been reported by Anderson (1993) and which is further supported by Paul et al. (2015), who note that the sea-ice areas around the Brunt Ice Shelf is the most active in the southern Weddell Sea, with an annual average polynya area of 3516 ± 1420 km². The reduced SIC here are also captured by our model, which is further described in Sect. 4.1.4.

$PIPSO_{25}$ values in the Amundsen Sea point to different scenarios. ~~While the~~ P_ZIPSO_{25} index ranges around 0.9 with ~~a slight decrease to a value of 0.3 in~~ the easterly, more distal location (Fig. 4a)~~, the~~ P_BIPSO_{25} index ~~is~~ generally lower~~,~~ ranging ~~around~~ 0.6 in the coastal area ~~and with a much steeper decline towards distal locations~~ to 0.2 (Fig. 4b). This difference between P_ZIPSO_{25} and P_BIPSO_{25} may be explained by the different source organisms biosynthesizing the individual phytoplankton biomarkers. While the main origin of HBI-trienes seems to be restricted to diatoms (Belt et al., 2017), brassicasterol is known to be produced by several algal

groups adapted to a wider range of sea surface conditions, such as dinoflagellates, diatoms, haptophytes, among others (Volkman, 2006).

4.1.3 TEX^{L}_{86} – and RI-OH' – derived temperatures

Isoprenoidal GDGTs are archaeal membrane lipid-derived proxies and valuable tools for reconstructing ocean temperatures (Schouten et al., 2002). These specific lipids, preserved in marine sediments, are sensitive to temperature change and relatively resistant to degradation processes (Huguet et al., 2008; Schouten et al., 2013). Schouten et al. (2002) found that the number of cyclopentane rings in sedimentary GDGTs is correlated with surface water temperatures and developed the first archaeal lipid paleothermometer TEX_{86}, a ratio of certain GDGTs, as a sea surface temperature (SST) proxy.

For a critical appraisal of the applicability and reliability of GDGT indices as temperature proxies in our investigated regions, we here make use of two temperature proxy approaches developed for the high latitude polar oceans: The TEX^{L}_{86} proxy by Kim et al. (2010) and the RI-OH' proxy by Lü et al. (2015), calculated and calibrated using Eq. 3 and 5, respectively.

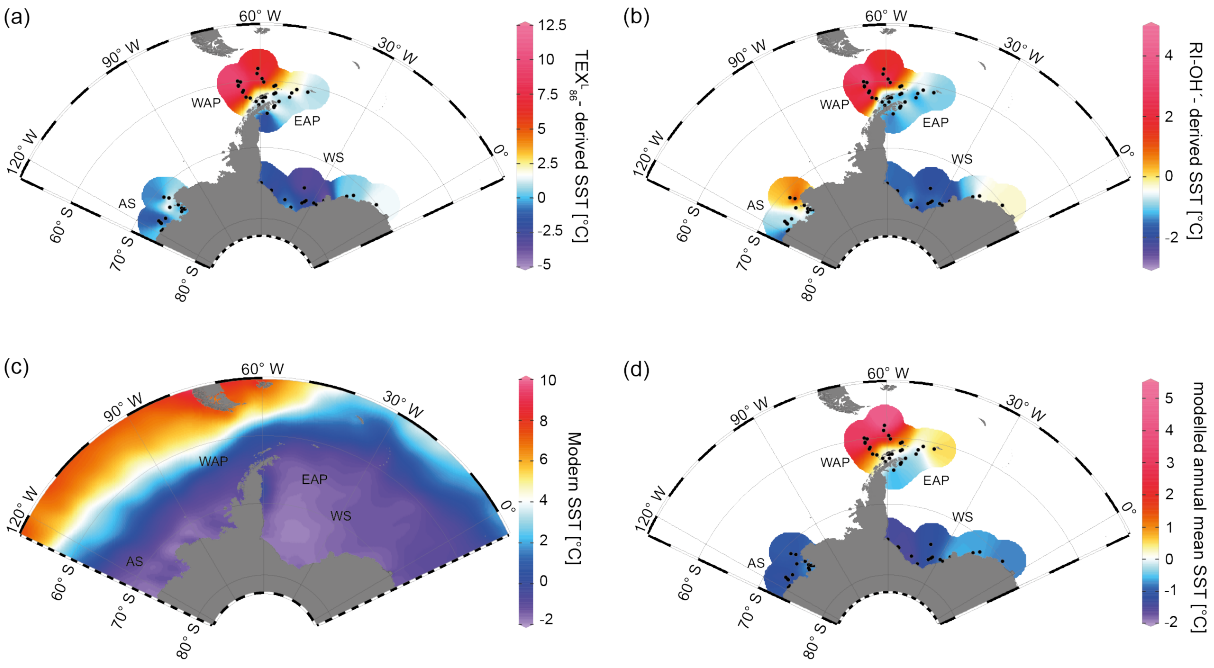

Fig. 5: Annual mean temperature distributions derived from (a) TEX^{L}_{86}, (b) RI-OH´, (c) WOA13 (Locarnini et al., 2013) and (d) model data in °C. AS: Amundsen Sea, WAP: West Antarctic Peninsula, EAP: East Antarctic Peninsula, WS: Weddell Sea.

427 The reconstructions represent annual mean ocean temperatures. In all samples, the BIT-
428 index (Eq. 6) is < 0.3, indicating no significant contribution of terrestrial input influencing the
429 distribution and hence applicability of GDGTs to estimate ocean temperatures. TEX^{L}_{86} and RI-
430 OH' both show a similar pattern, but different temperatures, ranging between -4.23 to +10.57
431 °C and -2.62 to +4.67 °C, respectively (Fig. 5a+b). At the West Antarctic Peninsula,
432 temperatures follow a northwest-southeast gradient with relatively higher temperatures in the
433 permanently ice-free Drake Passage and the continental slope, influenced by the ACC and
434 relatively warm CDW (Orsi et al., 1995; Rintoul et al., 2001). Temperatures decrease towards
435 the Bransfield Strait and the East Antarctic Peninsula, which are influenced by a seasonal sea-
436 ice cover and the relatively colder and highly saline TWW, branching off the Weddell Gyre
437 (Collares et al., 2018; Thompson et al., 2009). At the East Antarctic Peninsula, a southwest-
438 northeast gradient can be observed with relatively lower temperatures around the Larsen Ice
439 Shelf and higher temperatures towards the Powell Basin and the South Orkney Islands, towards
440 the North. These general temperature patterns align well with the decreasing sea-ice cover in
441 that area towards the North.

442 Absolute temperature estimates derived from the two paleothermometers show significantly
443 different ranges. While the TEX^{L}_{86} signal is reflecting temperatures in the Amundsen and
444 Weddell Seas quite well, it seems to be significantly warm-biased further to the North, in the
445 Drake Passage, with up to ~ 11 °C. This warm-biased TEX^{L}_{86} signal is a known caveat in that
446 area and is, among others, assumed to be connected to GDGTs produced by deep-dwelling
447 Euryarchaeota (Park et al., 2019), which have been reported in CDW (Alonso-Sáez et al., 2011)
448 and in deep waters of the Antarctic Polar Front (López-García et al., 2001). Interestingly, our
449 reconstructions suggest that the TEX^{L}_{86}-derived temperatures (Fig. 5a) are only warm-biased
450 in the relatively warmer Drake Passage but depict temperatures in the colder regions
451 (Amundsen and Weddell Seas) reasonably well or only slightly warm-biased, if compared to
452 the WOA13 temperatures (Fig. 5c).

Further to the South, in the Amundsen and Weddell Seas, temperatures are generally lower than at the Antarctic Peninsula. Samples from the Weddell Sea record a temperature decrease from east to west, which may reflect an eddy-driven route in the north-eastern corner of the Weddell Gyre carrying relatively warm, salty CDW, which then advects westward along the southern edge of the Weddell Gyre (Vernet et al., 2019). While the origin of GDGTs is not yet fully understood and still debated (Ho et al., 2014), the biosynthesis of intact polar lipid GDGTs in CDW, as just recently suggested by Spencer-Jones et al. (2020), might, however, support the hypothesis of advected CDW in that area. In the Amundsen Sea, relatively higher temperatures (~ 0.5 °C) at the sample locations in the north-eastern part of the embayment are reflected in the RI-OH'-derived temperatures but are not reflected in the TEX^{L}_{86}-based reconstruction.

4.1.4 Modelled SIC and SSTs

The global climate model setup AWI-ESM2 was used to simulate SSTs and SIC in the study area for modern conditions (1951-2014; Fig. 5d and 6, respectively). Modelled SIC indicate an absence of sea ice in the permanently ice-free Drake Passage (Fig. 6a-c) and a northwest-

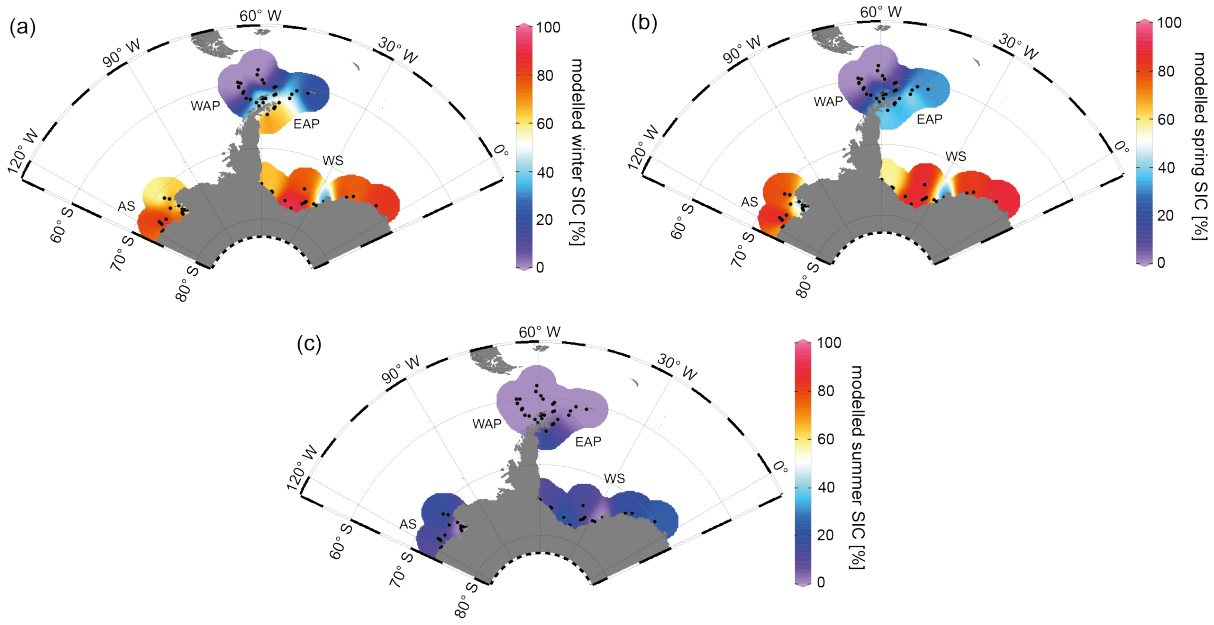

Fig. 6: Modelled SIC for (a) winter (JJA), (b) spring (SON) and (c) summer (DJF) in %. AS: Amundsen Sea, WAP: West Antarctic Peninsula, EAP: East Antarctic Peninsula, WS: Weddell Sea.

468 southeast gradient from the continental slope to the Bransfield Strait during winter and spring
469 (Fig. 6a+b) with the latter as being ice-free during summer (Fig. 6c). During all three seasons
470 (from winter through spring and summer), a southwest-northeast gradient at the East Antarctic
471 Peninsula can be observed, highlighting the decreasing sea-ice influence towards the Powell
472 Basin in the North. Absolute modelled SIC are decreasing from winter to summer, but still
473 underestimate SIC observed by satellites (Fig. 2). In the Amundsen and Weddell Seas, the
474 model shows a heavy sea-ice cover (~ 90 %) during winter and spring. Interestingly, modelled
475 SIC in the area in front of the Brunt Ice Shelf are as low as ~ 45 % (Fig. 6a+b), corresponding
476 well with the reduced $PIPSO_{25}$ value of ~ 0.51 % and may reflect the polynya conditions in that
477 region documented by Anderson (1993) and Paul et al. (2015). During summer, the model
478 suggests a reduction in SIC in the Amundsen and Weddell Seas to about 15-25 % (Fig. 6c),
479 slightly underestimating the satellite observations.
480 Modelled annual mean SSTs (Fig. 5d) are highest with up to 5 °C in the permanently ice-free
481 Drake Passage, influenced by the relatively warm ACC. Decreasing temperatures are simulated
482 towards the continental slope and the Bransfield Strait (~ 0.5-1 °C), coinciding with the
483 intensifying influence of sea-ice cover in that area. At the East Antarctic
484 Peninsula/northwestern Weddell Sea, the modelled SSTs show a southwest-northeast gradient
485 towards the Powell Basin with temperatures increasing from -0.5 °C in the South to 0.5 °C in
486 the North, aligning well with the other modelled records. In the Amundsen and Weddell Seas,
487 annual mean SSTs are negative, with temperatures from -0.5 to -1 °C.

5. Comparing biomarker data with satellite and numerical model data

Here, we discuss the advantages and caveats of the sea-ice biomarker $IPSO_{25}$ and the semi-quantitative sea-ice index $PIPSO_{25}$ by comparing the proxy data to satellite and numerical model data. The main ice algae bloom in the Southern Ocean occurs during spring, when temperatures increase, sea ice starts melting, which results in the release of nutrients and stratification of the water column and the increasing solar insulation stimulates the productivity of photosynthesizing organisms (Arrigo, 2017; Belt, 2018). The sea-ice biomarker $IPSO_{25}$ is hence commonly interpreted as a spring sea-ice indicator, which is why, in the following, we compare the biomarker-based sea-ice reconstructions to satellite-derived spring SIC and modelled spring SIC.

5.1 Comparison of proxy-based, modelled and observed sea-ice conditions

Our satellite-derived SIC represent monthly mean (spring) SIC averaged from 1978 to the individual year of sample retrieval. The herein modelled spring SIC cover a period from 1951 to 2014. When comparing sea-ice conditions estimated from sedimentary biomarker data (easily spanning decades to centuries, depending on sedimentation rates) with sea-ice conditions recorded by satellite observations (spanning ~ 40 years)~~,~~ and with modelled sea-ice conditions (spanning 63 years) the different time periods covered by the different methods need to be considered ~~and kept in mind~~ when interpreting the results. Vorrath et al. (2019) conducted radiocarbon dating on selected surface sediment samples from the Bransfield Strait, concluding that their biomarker data reflect the past two centuries. We hence note that biomarker data from the Antarctic Peninsula, which is affected by a very recent ice loss, may hence overestimate the sea-ice cover and underestimate ocean temperatures. Nonetheless we here correlate the biomarker data with satellite and model data to further investigate the quantitative significance of the sea ice proxy (Fig. 7). Following Esper and Gersonde (2014), who, assuming a non-linear

response of sea-ice diatom productivity to sea-ice dynamics, propose the ~~usage~~ of a polynomial regression instead of a linear correlation, we here use a polynomial regression (third degree).

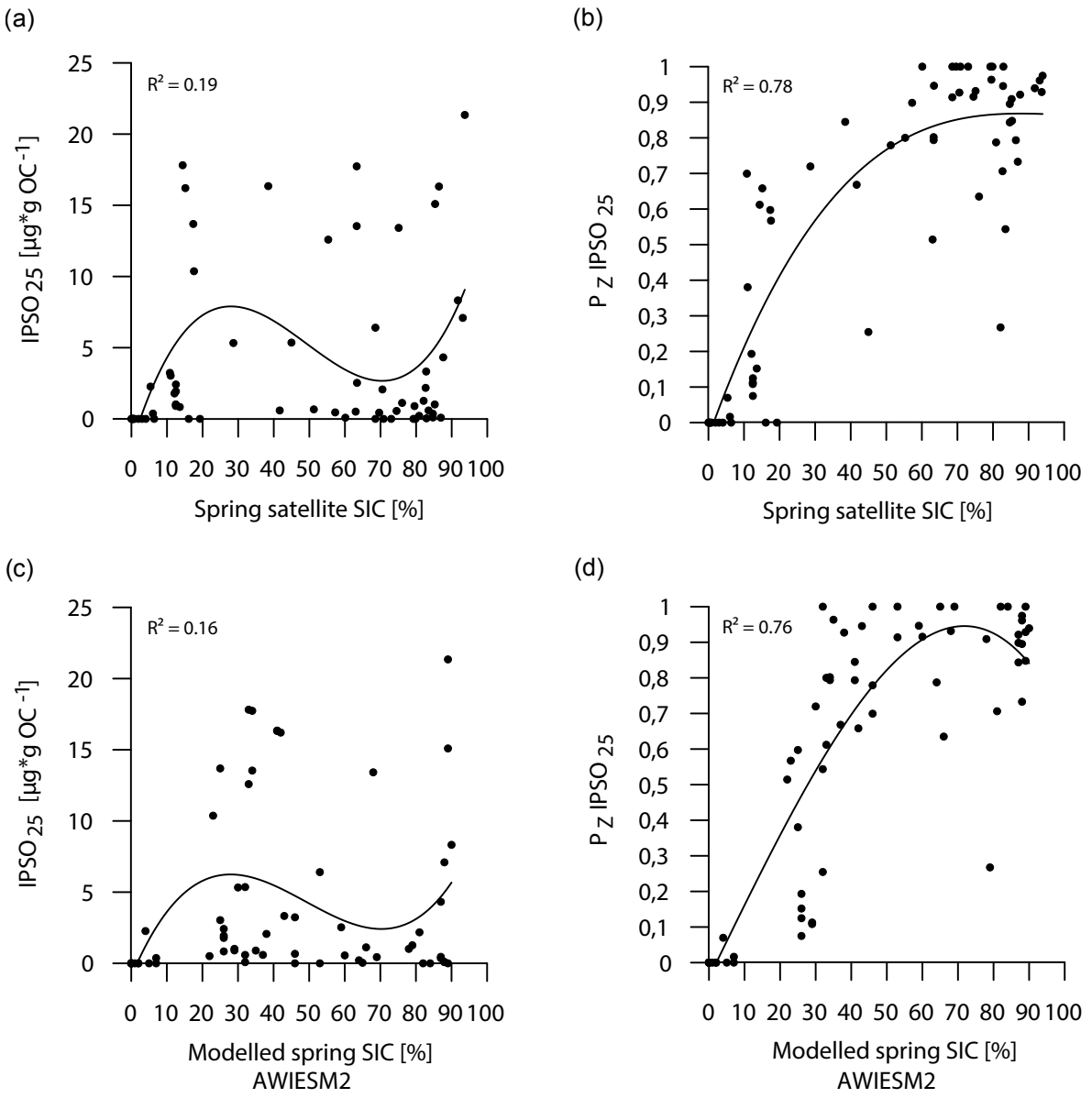

Fig. 7: Correlations of (a) $IPSO_{25}$ concentrations vs. spring satellite SIC, (b) P_ZIPSO_{25} values vs. spring satellite SIC, (c) $IPSO_{25}$ concentrations vs. modelled spring SIC and (d) P_ZIPSO_{25} values vs. modelled spring SIC. Coefficients of determination (R^2) are given for the respective regression lines.

$IPSO_{25}$ concentrations in the surface sediments around the Antarctic Peninsula exhibit similar trends as the satellite-derived and modelled SIC, while they differ significantly in the Amundsen and Weddell Seas, where high SIC are revealed by satellites and the model but $IPSO_{25}$ is very low concentrated. The relatively low $IPSO_{25}$ concentrations in these areas highlight the uncertainty when considering $IPSO_{25}$ as a sea-ice proxy alone, since such low

concentrations are not only observed under open water conditions, but also under a severe sea-ice cover. In this case, the low concentrations of $IPSO_{25}$ are the result of the latter, where limited light availability hinders ice algae growth, leading to an underestimation of sea-ice cover. As a result, $IPSO_{25}$ ~~and satellite/model~~ data show low correlations ($R^2 = 0.19$/$R^2 = 0.16$; Fig. 7a+c), requiring caution when interpreting $IPSO_{25}$ as a sea-ice proxy alone. As stated in earlier sections, the combination of $IPSO_{25}$ and a phytoplankton marker may prevent this ambiguity. The perennial sea-ice cover in the Amundsen and Weddell Seas is better represented by the P_ZIPSO_{25} values than by the sea-ice proxy alone. However, we note that ~~at the southern sampling sites,~~ the $PIPSO_{25}$ index ~~may not be able to further~~ resolve~~/detail~~ sea-ice concentrations higher than 50 % ~~reasonably well~~ (see Fig. S3). This may be an indicator for a threshold (here ~ 50 % SIC) where the growth of the HBI triene and $IPSO_{25}$ producing algae is limited.

In general, however, the P_ZIPSO_{25} values correlate much better with satellite/modelled SIC ($R^2 = 0.78$/$R^2 = 0.76$; Fig. 7b+d) than $IPSO_{25}$ concentrations. ~~For correlations~~ of satellite/model data with $PIPSO_{25}$ calculated using the HBI E-triene, brassicasterol and dinosterol, respectively, ~~we refer the reader to~~ Fig. S4. There are, however, also limitations in the semi-quantitative sea-ice index $PIPSO_{25}$, that need to be considered when interpreting this approach. A drawback may appear when the concentrations of the sea-ice proxy $IPSO_{25}$ and the phytoplankton marker are both low (due to unfavourable conditions for both ice algae as well as phytoplankton) or high (due to a significant seasonal shift in sea-ice cover and/or stable ice edge conditions), which may lead to similar $PIPSO_{25}$ values, although the sea-ice conditions are completely different from each other. This scenario was detected in five samples from the Weddell Sea (PS111/13-2, /15-1, /16-3, /29-3; /40-2; Fig. 3b+c), where $IPSO_{25}$ and the HBI Z-triene concentrations are close to the detection limit, while P_ZIPSO_{25} values are very low, suggesting a reduced sea-ice cover. Satellite and model data, however, show that these sample locations are influenced by heavy, perennial sea-ice conditions. We conclude that biomarker

546 concentrations of both biomarkers at or close to the detection limit, indicative of a severe ice
547 cover, need to be treated with caution. As mentioned above, we assigned a maximum P_ZIPSO_{25}
548 value of 1 to these samples and we note that such practice always needs to be made clear when
549 applying the $PIPSO_{25}$ approach.

550 The coupling of $IPSO_{25}$ with a phytoplankton marker, nonetheless, provides the more robust
551 and reliable sea-ice reconstructions. Regarding the above-mentioned ambiguities, we
552 recommend to not only calculate the $PIPSO_{25}$ index, but also consider individual biomarker
553 concentrations and, if possible, take other sea-ice measures, such as satellite data and/or well-
554 preserved diatom assemblage data (Lamping et al., 2020; Vorrath et al., 2019; 2020) into
555 account.

556

557 5.2 Temperature reconstructions

558 Concerning the different time frames covered by the proxy data and instrumental
559 observations, caution must be taken when comparing GDGT-derived ocean temperature
560 reconstructions (spanning decades to centuries) with modelled SSTs (spanning ~ 63 years) and
561 modern SSTs based on the WOA13 (covering the time period from 1955-2012; ~ 57 years).
562 Since it is still not fully understood whether GDGT-based temperature reconstructions
563 represent SSTs, near-surface or sub-surface ocean temperatures (Kalanetra et al., 2009; Kim et
564 al., 2012; Park et al., 2019) we here refer to ocean temperatures.

565 GDGT-derived temperatures, annual mean SSTs (depicted by the WOA13) and modelled
566 annual mean SSTs (Fig. 5a-d) show similar patterns at the Antarctic Peninsula and the
567 Amundsen and Weddell Seas. TEX^L_{86} values correlate reasonably well with modelled annual
568 mean SSTs ($R^2 = 0.71$; Fig. 8a). Following Park et al. (2019), stating that TEX^L_{86} values in the
569 Southern Ocean have a polynomial correlation with modern annual SSTs, we here also used a
570 polynomial correlation. As mentioned in Sect. 4.1.3, the temperatures are, however,
571 significantly warm-biased (up to ~ 7 °C higher), which may speculatively be attributable to

GDGT contributions of Euryarchaeota in CDW of the Antarctic Polar Front (Park et al., 2019). These findings are supported by a study by Spencer-Jones et al. (2020) in review, who found that GDGTs may be actively synthesized at CDW depths in the Amundsen Sea. They may hence be a significant source of isoprenoidal GDGTs within the sediments in that area.

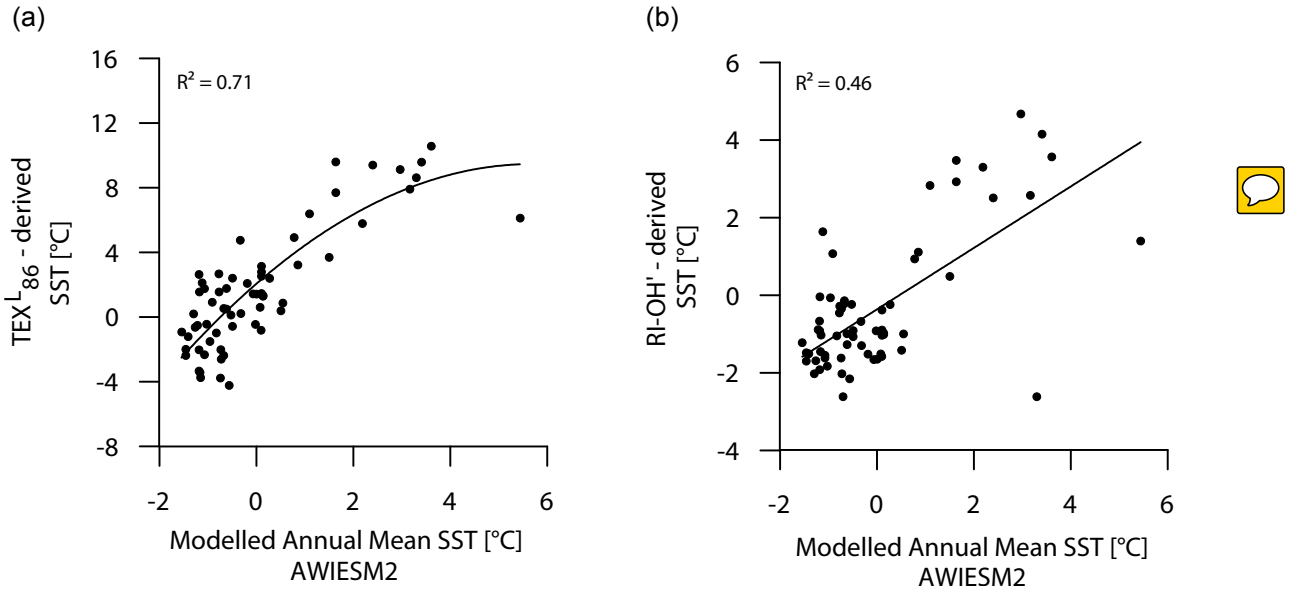

Fig. 8: Correlations of (a) TEX^L_{86}-derived temperatures vs. modelled annual mean SSTs and (b) RI-OH'-derived temperatures vs. modelled annual mean SSTs. Coefficients of determination (R^2) are given for the respective regression lines.

The correlation with RI-OH'-derived temperatures is slightly lower (R^2 = 0.46; Fig. 8b), the temperature ranges of RI-OH' are, however, much more realistic (from -3 to 5 °C), supporting the study by Park et al. (2019). The addition of OH-isoGDGTs in the temperature index is a promising step towards high latitude temperature reconstructions and may improve our understanding of the temperature responses of archaeal membranes in Southern Ocean waters (Fietz et al., 2020; Park et al., 2019). Clearly, more data – ideally obtained from sediment traps, surface samples as well as longer sediment cores – and calibration studies will help to further elucidate the applicability of this approach.

6. The role of platelet ice for $IPSO_{25}$ production

Platelet ice formation plays an important role in sea-ice generation along some coastal regions of Antarctica (Hoppmann et al., 2015; 2020; Lange et al., 1989; Langhorne et al., 2015). In these regions, High Saline Shelf Water (HSSW) flows into sub-ice shelf cavities of Antarctica´s continental shelves, initiating basal melt of the adjacent ice shelves (Fig. 9). The surrounding water is cooled and freshened and is then transported towards the surface, where the pressure relief can cause this water, called Ice Shelf Water (ISW), to be supercooled (Foldvik and Kvinge, 1974). The temperature of the supercooled ISW is potentially below the in-situ freezing point, which may eventually cause the formation of ice platelets that accumulate under landfast ice attached to adjacent ice shelves (Fig. 9; Holland et al., 2007; Hoppmann et al., 2015; 2020).

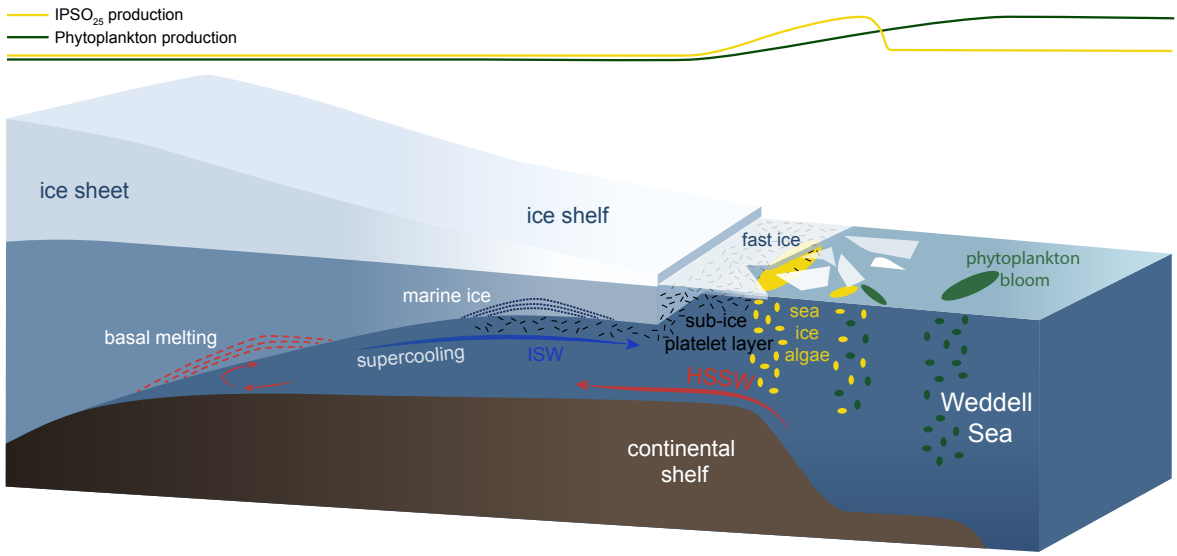

Fig. 9: Schematic illustration of the formation of platelet ice and the main production areas of sea ice algae producing $IPSO_{25}$ (yellow ovals) and phytoplankton (green ovals), also displayed by yellow and green curves at the top. HSSW: High Saline Shelf Water, ISW: Ice Shelf Water. Schematic modified after Scambos et al. (2017).

The sympagic, tube-dwelling, diatom *B. adeliensis* is a common constituent of Antarctic sea ice, preferably flourishing in the relatively open channels of sub-ice platelet layers in near-shore locations covered by fast ice (Medlin, 1990; Riaux-Gobin and Poulin, 2004). Based on investigations of sea-ice samples from the Southern Ocean, Belt et al. (2016) detected this

599 diatom species to be a source of the HBI diene $IPSO_{25}$, which, according to its habitat, led to
600 the assumption of the sea-ice proxy being a potential indicator for the presence of platelet ice.
601 As stated above, *B. adeliensis* is not confined to platelet ice, but is also observed in bottom ice
602 and described as well adapted to changes in the texture of sea ice during ice melt (Riaux-Gobin
603 et al., 2013).

604 In an attempt to elucidate the relationship of $IPSO_{25}$ and platelet ice more clearly, we here
605 regard our data in connection to observed platelet ice occurrences.

606 Elevated $IPSO_{25}$ concentrations in front of the Larsen Ice Shelves at the East Antarctic
607 Peninsula could be linked to several processes. So far, it is hard to differentiate between in-situ
608 $IPSO_{25}$ production or allochthonous input of $IPSO_{25}$ from drift ice. According to Langhorne et
609 al. (2015), sea-ice cores retrieved from that area did not incorporate platelet ice. The high
610 $IPSO_{25}$ concentrations could hence be explicable by either drift ice by the Weddell Gyre or by
611 bottom ice production. We do, however, note that our samples reflect much longer time frames
612 than the sea-ice samples investigated by Langhorne et al. (2015). The lack of platelet ice
613 observed in their investigated sea-ice cores does not rule out the former presence of platelet ice,
614 which may be captured in our investigated sediment samples, covering a much longer time
615 interval.

616 There are several previous studies on $IPSO_{25}$ which report a close connection of the proxy
617 to proximal, coastal locations and polynyas in the seasonal ice zone (i.e., Collins et al., 2013;
618 Smik et al., 2016). They do not, however, discuss the relation to adjacent ice shelves as possible
619 "platelet ice factories". We note that the core locations investigated by Smik et al. (2016) are
620 in the vicinity of the Moscow University Ice Shelf, where Langhorne et al. (2015) did not
621 observe platelet ice within sea-ice cores. Hoppmann et al. (2020), however, report on a sea-ice
622 core from that area, incorporating platelet ice. The different observations by Langhorne et al.
623 (2015) and Hoppmann et al. (2020) show how variable the occurrence of platelet ice can be.

The absence of $IPSO_{25}$ in the Amundsen Sea (Fig. 3b; AS) might in turn be explicable by the absence of platelet ice in that region. The Amundsen Sea shelf is classified as a warm shelf (Thompson et al., 2018) and characterized by the upwelling of warm CDW (Schmidtko et al., 2014), hindering the formation of ISW and making the presence of platelet ice in recent conditions highly unlikely (Hoppmann et al., 2020). This theory is also supported by Langhorne et al. (2015), stating that platelet ice formation is not observed, where thinning from basal melting of ice shelves is believed to be greatest, which applies to the warm shelf of the Amundsen Sea (Thompson et al., 2018). Accordingly, if the formation and accumulation of platelet ice – up to a certain degree – is indicative of basal ice shelf melting on fresh shelves (Hoppmann et al., 2015; Thompson et al., 2018), high $IPSO_{25}$ concentrations determined in marine sediments may hence serve as indicator of past basal melting processes and associated ice shelf dynamics. This may, however, only be true up to a certain threshold where platelet ice formation is diminished/hampered due to warm oceanic conditions leading to a too intense basal melting (Langhorne et al., 2015).

While using $IPSO_{25}$ as a sea-ice proxy in Antarctica, it is hence important to also consider regional platelet ice formation processes as these may affect the $IPSO_{25}$ budget. Determining thresholds associated with platelet ice formation is challenging, therefore, further investigations, such as in-situ measurements of $IPSO_{25}$ concentrations in platelet ice or culture experiments in home laboratories are needed to better depict the connection between $IPSO_{25}$ and platelet ice formation (and ice shelf basal melting).

7. Conclusion

Biomarker analyses focusing on $IPSO_{25}$, HBI-trienes, phytosterols and GDGTs, in surface sediment samples from the continental shelves off West Antarctica were investigated to depict recent sea surface and temperature conditions in this climate sensitive region. Proxy-based reconstructions of the sea surface conditions were compared to (1) satellite observations and (2) estimated sea-ice patterns and SSTs deduced from model data. The semi-quantitative sea-ice index $PIPSO_{25}$, combining the sea-ice proxy $IPSO_{25}$ with an open-water phytoplankton marker, yielded reasonably good correlations with satellite observations and numerical model results, while correlations with the sea-ice proxy $IPSO_{25}$ alone are rather low. Minimum concentrations of both biomarkers, used for the $PIPSO_{25}$ calculations, however, may lead to ambiguous interpretations and significant underestimations of sea-ice conditions. The combination of different sea-ice measures when interpreting biomarker data should hence be strived for.

The presumed relationship between $IPSO_{25}$ and platelet ice formation in connection to basal melting of ice shelves is supported by our data, showing high $IPSO_{25}$ concentrations in areas where platelet ice formation has previously been reported and low $IPSO_{25}$ concentrations where no platelet ice formation is occurring. Oceanic conditions and the intensity of basal melting, however, need to be considered when using $IPSO_{25}$ as an indirect indicator for basal melting processes and associated ice shelf dynamics.

Temperature reconstructions based on TEX^{L}_{86} and RI-OH' paleothermometers show similar patterns, but different absolute temperatures. While TEX^{L}_{86}-derived temperatures are significantly warm-biased, the RI-OH'-derived temperatures are proven more realistic, when compared to temperature data based on the WOA13 and modelled annual mean SSTs. Further investigations of HBI synthesis, transport, sedimentation and preservation within the sediments as well as the composition of its sources habitat (bottom ice, platelet ice, brine channels) and

its connection to platelet ice formation via in situ or laboratory measurements are required to better constrain the proxy´s potential as a robust sea-ice biomarker.

Data availability

Datasets related to this article can be found online on *PANGAEA Data Publisher for Earth & Environmental Science* (doi: in prep).

Author contribution

N.L. and J.M. designed the concept of the study. N.L. carried out biomarker experiments. X.S and G.L. developed the model code and X.S. performed the simulations. C.H. provided the satellite data. N.L. prepared the manuscript and visualizations with contributions from all co-authors.

Competing interests

The authors declare that they have no conflict of interest.

Acknowledgements

Denise Diekstall, Mandy Kuck and Jonas Haase are kindly acknowledged for laboratory support. We thank the captains, crews and science parties of *RV Polarstern* cruises PS69, PS97, PS104, PS111 and PS118. Especially Frank Niessen, Sabine Hanisch and Michael Schreck are thanked for their support during PS118. Simon Belt is acknowledged for providing the 7-HND internal standard for HBI quantification. N.L., M.-E.V. and J.M. were funded through the Helmholtz Research Grant VH-NG-1101.

691 **References**

692 Abernathey, R. P., Cerovecki, I., Holland, P. R., Newsom, E., Mazloff, M., and Talley, L. D.:
693 Water-mass transformation by sea ice in the upper branch of the Southern Ocean
694 overturning, Nature Geoscience, 9, 596-601, 2016.

695 Allen, C. S., Pike, J., and Pudsey, C. J.: Last glacial–interglacial sea-ice cover in the SW
696 Atlantic and its potential role in global deglaciation, Quaternary Science Reviews, 30, 2446-
697 2458, 2011.

698 Alonso-Sáez, L., Andersson, A., Heinrich, F., and Bertilsson, S.: High archaeal diversity in
699 Antarctic circumpolar deep waters, Environmental microbiology reports, 3, 689-697, 2011.

700 Anderson, P. S.: Evidence for an Antarctic winter coastal polynya, Antarctic science, 5, 221-
701 226, 1993.

702 Armand, L. K., and Leventer, A.: Palaeo sea ice distribution–reconstruction and palaeoclimatic
703 significance, Sea ice—an introduction to its physics, biology, chemistry, and geology, 333-
704 372, 2003.

705 Arrigo, K. R., Worthen, D. L., Lizotte, M. P., Dixon, P., and Dieckmann, G.: Primary
706 production in Antarctic sea ice, Science, 276, 394-397, 1997.

707 Arrigo, K. R.: Sea ice as a habitat for primary producers, Sea ice, 352-369, 2017.

708 Barbara, L., Crosta, X., Massé, G., and Ther, O.: Deglacial environments in eastern Prydz Bay,
709 East Antarctica, Quaternary Science Reviews, 29, 2731-2740, 2010.

710 Barbara, L., Crosta, X., Schmidt, S., and Massé, G.: Diatoms and biomarkers evidence for major
711 changes in sea ice conditions prior the instrumental period in Antarctic Peninsula,
712 Quaternary Science Reviews, 79, 99-110, 2013.

713 Belt, S. T., Allard, W. G., Massé, G., Robert, J.-M., and Rowland, S. J.: Highly branched
714 isoprenoids (HBIs): identification of the most common and abundant sedimentary isomers,
715 Geochimica et Cosmochimica Acta, 64, 3839-3851, 2000.

716 Belt, S. T., and Müller, J.: The Arctic sea ice biomarker IP_{25}: a review of current understanding,
717 recommendations for future research and applications in palaeo sea ice reconstructions,
718 Quaternary Science Reviews, 79, 9-25, 2013.
719 Belt, S. T., Brown, T. A., Ampel, L., Cabedo-Sanz, P., Fahl, K., Kocis, J. J., Masse, G.,
720 Navarro-Rodriguez, A., Ruan, J., and Xu, Y.: An inter-laboratory investigation of the Arctic
721 sea ice biomarker proxy IP_{25} in marine sediments: key outcomes and recommendations,
722 Climate of the Past., 10, 155-166, 2014.
723 Belt, S. T., Cabedo-Sanz, P., Smik, L., Navarro-Rodriguez, A., Berben, S. M. P., Knies, J., and
724 Husum, K.: Identification of paleo Arctic winter sea ice limits and the marginal ice zone:
725 Optimised biomarker-based reconstructions of late Quaternary Arctic sea ice, Earth and
726 Planetary Science Letters, 431, 127-139, 2015.
727 Belt, S. T., Smik, L., Brown, T. A., Kim, J. H., Rowland, S. J., Allen, C. S., Gal, J. K., Shin, K.
728 H., Lee, J. I., and Taylor, K. W. R.: Source identification and distribution reveals the
729 potential of the geochemical Antarctic sea ice proxy $IPSO_{25}$, Nature Communications, 7,
730 12655, https://doi.org/10.1038/ncomms12655, 2016.
731 Belt, S. T., Brown, T. A., Smik, L., Tatarek, A., Wiktor, J., Stowasser, G., Assmy, P., Allen, C.
732 S., and Husum, K.: Identification of C_{25} highly branched isoprenoid (HBI) alkenes in
733 diatoms of the genus Rhizosolenia in polar and sub-polar marine phytoplankton, Organic
734 Geochemistry, 110, 65-72, 2017.
735 Belt, S. T.: Source-specific biomarkers as proxies for Arctic and Antarctic sea ice, Organic
736 Geochemistry, 125, 277-298, 2018.
737 Berger, A.: Long-term variations of daily insolation and Quaternary climatic changes, Journal
738 of the atmospheric sciences, 35, 2362-2367, 1978.
739 Boon, J. J., Rijpstra, W. I. C., de Lange, F., De Leeuw, J., Yoshioka, M., and Shimizu, Y.:
740 Black Sea sterol—a molecular fossil for dinoflagellate blooms, Nature, 277, 125-127, 1979.

741 Cavalieri, D., Parkinson, C., Gloersen, P., and Zwally, H.: Sea ice concentrations from Nimbus-
742 7 SMMR and DMSP SSM/I passive microwave data, National Snow and Ice Data Center,
743 Boulder, Colorado, USA, 1996.
744 Collares, L. L., Mata, M. M., Kerr, R., Arigony-Neto, J., and Barbat, M. M.: Iceberg drift and
745 ocean circulation in the northwestern Weddell Sea, Antarctica, Deep Sea Research Part II:
746 Topical Studies in Oceanography, 149, 10-24, 2018.
747 Colleoni, F., De Santis, L., Siddoway, C. S., Bergamasco, A., Golledge, N. R., Lohmann, G.,
748 Passchier, S., and Siegert, M. J.: Spatio-temporal variability of processes across Antarctic
749 ice-bed–ocean interfaces, Nature Communications, 9, 2289, https://doi.org/10.1038/s41467-
750 018-04583-0, 2018.
751 Collins, L. G., Allen, C. S., Pike, J., Hodgson, D. A., Weckström, K., and Massé, G.: Evaluating
752 highly branched isoprenoid (HBI) biomarkers as a novel Antarctic sea-ice proxy in deep
753 ocean glacial age sediments, Quaternary Science Reviews, 79, 87-98, 2013.
754 Comiso, J. C., Gersten, R. A., Stock, L. V., Turner, J., Perez, G. J., and Cho, K.: Positive Trend
755 in the Antarctic Sea Ice Cover and Associated Changes in Surface Temperature, Journal of
756 Climate, 30, 2251-2267, 2017.
757 Crosta, X., Pichon, J. J., and Burckle, L.: Application of modern analog technique to marine
758 Antarctic diatoms: Reconstruction of maximum sea-ice extent at the Last Glacial Maximum,
759 Paleoceanography and Paleoclimatology, 13, 284-297, 1998.
760 Danilov, S., Sidorenko, D., Wang, Q., and Jung, T.: The Finite-volumE Sea ice–Ocean Model
761 (FESOM2), Geosci. Model Dev., 10, 765-789, 2017.
762 Deacon, G. R. E.: The Weddell Gyre, Deep Sea Research Part A. Oceanographic Research
763 Papers, 26, 981-995, 1979.
764 Denis, D., Crosta, X., Barbara, L., Massé, G., Renssen, H., Ther, O., and Giraudeau, J.: Sea ice
765 and wind variability during the Holocene in East Antarctica: insight on middle–high latitude
766 coupling, Quaternary Science Reviews, 29, 3709-3719, 2010.

767 Dorschel, B.: The Expedition PS118 of the Research Vessel POLARSTERN to the Weddell
768 Sea in 2019, Berichte zur Polar-und Meeresforschung = Reports on polar and marine
769 research, 735, 2019.
770 Doty, M. S., and Oguri, M.: The island mass effect, ICES Journal of Marine Science, 22, 33-
771 37, 1956.
772 Esper, O., and Gersonde, R.: New tools for the reconstruction of Pleistocene Antarctic sea ice,
773 Palaeogeography, Palaeoclimatology, Palaeoecology, 399, 260-283, 2014.
774 Etourneau, J., Collins, L. G., Willmott, V., Kim, J.-H., Barbara, L., Leventer, A., Schouten, S.,
775 Damsté, J. S., Bianchini, A., and Klein, V.: Holocene climate variations in the western
776 Antarctic Peninsula: evidence for sea ice extent predominantly controlled by changes in
777 insolation and ENSO variability, Climate of the Past, 9, 1431-1446, 2013.
778 Fahl, K., and Stein, R.: Modern seasonal variability and deglacial/Holocene change of central
779 Arctic Ocean sea-ice cover: new insights from biomarker proxy records, Earth and Planetary
780 Science Letters, 351, 123-133, 2012.
781 Fetterer, F., Knowles, K., Meier, W., Savoie, M., Windnagel, A.K., 2016. Updated Daily. Sea
782 Ice Index, Version 2. [Median Sea Ice Extent 1981-2010]. NSIDC: National Snow and Ice
783 Data Center, Boulder, Colorado USA. https://doi.org/10.7265/N5736NV7 [24 July 2017].
784 Fietz, S., Huguet, C., Rueda, G., Hambach, B., and Rosell-Melé, A.: Hydroxylated isoprenoidal
785 GDGTs in the Nordic Seas, Marine Chemistry, 152, 1-10, 2013.
786 Fietz, S., Ho, S., and Huguet, C.: Archaeal Membrane Lipid-Based Paleothermometry for
787 Applications in Polar Oceans, Oceanography, 33, 104-114, 2020.
788 Foldvik, A., and Kvinge, T.: Conditional instability of sea water at the freezing point, Deep Sea
789 Research and Oceanographic Abstracts, 21, 169-174, 1974.
790 Gersonde, R., and Zielinski, U.: The reconstruction of late Quaternary Antarctic sea-ice
791 distribution—the use of diatoms as a proxy for sea-ice, Palaeogeography,
792 Palaeoclimatology, Palaeoecology, 162, 263-286, 2000.

Gohl, K.: The expedition ANTARKTIS-XXIII/4 of the research vessel Polarstern in 2006, Berichte zur Polar-und Meeresforschung (Reports on Polar and Marine Research), 557, 2007.

Gohl, K.: The Expedition PS104 of the Research Vessel POLARSTERN to the Amundsen Sea in 2017, Berichte zur Polar-und Meeresforschung = Reports on polar and marine research, 712, 2017.

Hancke, K., Lund-Hansen, L. C., Lamare, M. L., Højlund Pedersen, S., King, M. D., Andersen, P., and Sorrell, B. K.: Extreme low light requirement for algae growth underneath sea ice: A case study from Station Nord, NE Greenland, Journal of Geophysical Research: Oceans, 123, 985-1000, 2018.

Harms, S., Fahrbach, E., and Strass, V. H.: Sea ice transports in the Weddell Sea, Journal of Geophysical Research: Oceans, 106, 9057-9073, 2001.

Ho, S. L., Mollenhauer, G., Fietz, S., Martínez-Garcia, A., Lamy, F., Rueda, G., Schipper, K., Méheust, M., Rosell-Melé, A., Stein, R., and Tiedemann, R.: Appraisal of TEX_{86} and thermometries in subpolar and polar regions, Geochimica et Cosmochimica Acta, 131, 213-226, 2014.

Hobbs, W. R., Massom, R., Stammerjohn, S., Reid, P., Williams, G., and Meier, W.: A review of recent changes in Southern Ocean sea ice, their drivers and forcings, Global and Planetary Change, 143, 228-250, 2016.

Holland, P. R., Feltham, D. L., and Jenkins, A.: Ice shelf water plume flow beneath Filchner-Ronne Ice Shelf, Antarctica, Journal of Geophysical Research: Oceans, 112, https://doi.org/10.1029/2006JC003915, 2007.

Hopmans, E. C., Weijers, J. W., Schefuß, E., Herfort, L., Damsté, J. S. S., and Schouten, S.: A novel proxy for terrestrial organic matter in sediments based on branched and isoprenoid tetraether lipids, Earth and Planetary Science Letters, 224, 107-116, 2004.

Hoppmann, M., Nicolaus, M., Paul, S., Hunkeler, P. A., Heinemann, G., Willmes, S., Timmermann, R., Boebel, O., Schmidt, T., and Kühnel, M.: Ice platelets below Weddell Sea landfast sea ice, Annals of Glaciology, 56, 175-190, 2015.

Hoppmann, M., Richter, M. E., Smith, I. J., Jendersie, S., Langhorne, P. J., Thomas, D. N., and Dieckmann, G. S.: Platelet ice, the Southern Ocean's hidden ice: a review, Annals of Glaciology, 1-28, 2020.

Huguet, C., de Lange, G. J., Gustafsson, Ö., Middelburg, J. J., Damsté, J. S. S., and Schouten, S.: Selective preservation of soil organic matter in oxidized marine sediments (Madeira Abyssal Plain), Geochimica et Cosmochimica Acta, 72, 6061-6068, 2008.

Iacono, M. J., Delamere, J. S., Mlawer, E. J., Shephard, M. W., Clough, S. A., and Collins, W. D.: Radiative forcing by long-lived greenhouse gases: Calculations with the AER radiative transfer models, Journal of Geophysical Research: Atmospheres, 113, https://doi.org/10.1029/2008JD009944, 2008.

Jacobs, S. S., Jenkins, A., Giulivi, C. F., and Dutrieux, P.: Stronger ocean circulation and increased melting under Pine Island Glacier ice shelf, Nature Geoscience, 4, 519-523, 2011.

Jenkins, A., and Jacobs, S.: Circulation and melting beneath George VI ice shelf, Antarctica, Journal of Geophysical Research: Oceans, 113, https://doi.org/10.1029/2007JC004449, 2008.

Johns, L., Wraige, E., Belt, S., Lewis, C., Massé, G., Robert, J.-M., and Rowland, S.: Identification of a C_{25} highly branched isoprenoid (HBI) diene in Antarctic sediments, Antarctic sea-ice diatoms and cultured diatoms, Organic Geochemistry, 30, 1471-1475, 1999.

Kalanetra, K. M., Bano, N., and Hollibaugh, J. T.: Ammonia-oxidizing Archaea in the Arctic Ocean and Antarctic coastal waters, Environmental Microbiology, 11, 2434-2445, 2009.

Kim, J.-H., Van der Meer, J., Schouten, S., Helmke, P., Willmott, V., Sangiorgi, F., Koç, N., Hopmans, E. C., and Damsté, J. S. S.: New indices and calibrations derived from the

distribution of crenarchaeal isoprenoid tetraether lipids: Implications for past sea surface temperature reconstructions, Geochimica et Cosmochimica Acta, 74, 4639-4654, 2010.

Kim, J.-H., Crosta, X., Willmott, V., Renssen, H., Bonnin, J., Helmke, P., Schouten, S., and Sinninghe Damsté, J. S.: Holocene subsurface temperature variability in the eastern Antarctic continental margin, Geophysical Research Letters, 39, https://doi.org/10.1029/2012GL051157, 2012.

Klinck, J. M., Hofmann, E. E., Beardsley, R. C., Salihoglu, B., and Howard, S.: Water-mass properties and circulation on the west Antarctic Peninsula Continental Shelf in Austral Fall and Winter 2001, Deep Sea Research Part II: Topical Studies in Oceanography, 51, 1925-1946, 2004.

Köhler, P., Nehrbass-Ahles, C., Schmitt, J., Stocker, T. F., and Fischer, H.: A 156 kyr smoothed history of the atmospheric greenhouse gases CO_2, CH_4, and N_2O and their radiative forcing, Earth Syst. Sci. Data, 9, 363-387, 2017.

Lamping, N., Müller, J., Esper, O., Hillenbrand, C.-D., Smith, J. A., and Kuhn, G.: Highly branched isoprenoids reveal onset of deglaciation followed by dynamic sea-ice conditions in the western Amundsen Sea, Antarctica, Quaternary Science Reviews, 228, https://doi.org/10.1016/j.quascirev.2019.106103, 2020.

Lange, M., Ackley, S., Wadhams, P., Dieckmann, G., and Eicken, H.: Development of sea ice in the Weddell Sea, Annals of Glaciology, 12, 92-96, 1989.

Langhorne, P., Hughes, K., Gough, A., Smith, I., Williams, M., Robinson, N., Stevens, C., Rack, W., Price, D., and Leonard, G.: Observed platelet ice distributions in Antarctic sea ice: An index for ocean-ice shelf heat flux, Geophysical Research Letters, 42, 5442-5451, 2015.

Leventer, A.: The fate of Antarctic “sea ice diatoms” and their use as paleoenvironmental indicators, Antarctic sea ice. Biological processes, interactions and variability, 121-137, 1998.

Liu, J., Curry, J. A., and Martinson, D. G.: Interpretation of recent Antarctic sea ice variability, Geophysical Research Letters, 31, https://doi.org/10.1029/2003GL018732, 2004.

Locarnini, R. A., Mishonov, A. V., Antonov, J. I., Boyer, T. P., Garcia, H. E., Baranova, O. K., Zweng, M. M., Paver, C. R., Reagan, J. R., and Johnson, D. R.: World ocean atlas 2013. Volume 1, Temperature, NOAA Atlas NESDIS 73, 40 pp., doi: 10.7289/V55X26VD, 2013.

Lohmann, G., Butzin, M., Eissner, N., Shi, X., and Stepanek, C.: Abrupt climate and weather changes across time scales, Paleoceanography and Paleoclimatology, 35, https://doi.org/10.1029/2019PA003782, 2020.

López-García, P., Rodriguez-Valera, F., Pedrós-Alió, C., and Moreira, D.: Unexpected diversity of small eukaryotes in deep-sea Antarctic plankton, Nature, 409, 603-607, 2001.

Lorenz, S. J., and Lohmann, G.: Acceleration technique for Milankovitch type forcing in a coupled atmosphere-ocean circulation model: method and application for the Holocene, Climate Dynamics, 23, 727-743, 2004.

Lott, F.: Alleviation of stationary biases in a GCM through a mountain drag parameterization scheme and a simple representation of mountain lift forces, Monthly weather review, 127, 788-801, 1999.

Loveland, T. R., Reed, B. C., Brown, J. F., Ohlen, D. O., Zhu, Z., Yang, L., and Merchant, J. W.: Development of a global land cover characteristics database and IGBP DISCover from 1 km AVHRR data, Int. J. Remote Sens., 21, 1303-1330, 2000.

Lü, X., Liu, X.-L., Elling, F. J., Yang, H., Xie, S., Song, J., Li, X., Yuan, H., Li, N., and Hinrichs, K.-U.: Hydroxylated isoprenoid GDGTs in Chinese coastal seas and their potential as a paleotemperature proxy for mid-to-low latitude marginal seas, Organic Geochemistry, 89-90, 31-43, 2015.

Massé, G., Belt, S. T., Crosta, X., Schmidt, S., Snape, I., Thomas, D. N., and Rowland, S. J.: Highly branched isoprenoids as proxies for variable sea ice conditions in the Southern Ocean, Antarctic Science, 23, 487-498, 2011.

Massom, R. A., Scambos, T. A., Bennetts, L. G., Reid, P., Squire, V. A., and Stammerjohn, S. E.: Antarctic ice shelf disintegration triggered by sea ice loss and ocean swell, Nature, 558, 383-389, 2018.

Medlin, L.: Berkeleya spp. from Antarctic waters, including Berkeleya adeliensis, sp. nov., a new tube dwelling diatom from the undersurface of sea-ice, Beihefte zur Nova Hedwigia, 100, 77-89, 1990.

Meredith, M. P., Woodworth, P. L., Chereskin, T. K., Marshall, D. P., Allison, L. C., Bigg, G. R., Donohue, K., Heywood, K. J., Hughes, C. W., and Hibbert, A.: Sustained monitoring of the Southern Ocean at Drake Passage: Past achievements and future priorities, Reviews of Geophysics, 49, https://doi.org/10.1029/2010RG000348, 2011.

Meyers, P. A.: Organic geochemical proxies of paleoceanographic, paleolimnologic, and paleoclimatic processes, Organic geochemistry, 27, 213-250, 1997.

Moore, J. K., and Abbott, M. R.: Surface chlorophyll concentrations in relation to the Antarctic Polar Front: seasonal and spatial patterns from satellite observations, Journal of Marine Systems, 37, 69-86, 2002.

Müller, J., Wagner, A., Fahl, K., Stein, R., Prange, M., and Lohmann, G.: Towards quantitative sea ice reconstructions in the northern North Atlantic: A combined biomarker and numerical modelling approach, Earth and Planetary Science Letters, 306, 137-148, 2011.

Müller, J., and Stein, R.: High-resolution record of late glacial and deglacial sea ice changes in Fram Strait corroborates ice–ocean interactions during abrupt climate shifts, Earth and Planetary Science Letters, 403, 446-455, 2014.

Nicholls, K. W., Østerhus, S., Makinson, K., Gammelsrød, T., and Fahrbach, E.: Ice-ocean processes over the continental shelf of the southern Weddell Sea, Antarctica: A review, Reviews of Geophysics, 47, https://doi.org/10.1029/2007RG000250, 2009.

Nichols, P. D., Palmisano, A. C., Volkman, J. K., Smith, G. A., and White, D. C.: Occurrence of an isoprenoid C_{25} diunasaturated alkene and high neutral lipid content in Antarctic sea-ice diatom communities 1, Journal of Phycology, 24, 90-96, 1988.

Nielsdóttir, M. C., Bibby, T. S., Moore, C. M., Hinz, D. J., Sanders, R., Whitehouse, M., Korb, R., and Achterberg, E. P.: Seasonal and spatial dynamics of iron availability in the Scotia Sea, Marine Chemistry, 130, 62-72, 2012.

Nolting, R., De Baar, H., Van Bennekom, A., and Masson, A.: Cadmium, copper and iron in the Scotia Sea, Weddell Sea and Weddell/Scotia confluence (Antarctica), Marine Chemistry, 35, 219-243, 1991.

Orsi, A. H., Whitworth III, T., and Nowlin Jr, W. D.: On the meridional extent and fronts of the Antarctic Circumpolar Current, Deep Sea Research Part I: Oceanographic Research Papers, 42, 641-673, 1995.

Otto-Bliesner, B., Brady, E., Zhao, A., Brierley, C., Axford, Y., Capron, E., Govin, A., Hoffman, J., Isaacs, E., and Kageyama, M.: Large-scale features of Last Interglacial climate: Results from evaluating the lig127k simulations for CMIP6-PMIP4, Climate of the Past, 17, 63-94, 2021.

Otto-Bliesner, B. L., Braconnot, P., Harrison, S. P., Lunt, D. J., Abe-Ouchi, A., Albani, S., Bartlein, P. J., Capron, E., Carlson, A. E., and Dutton, A.: The PMIP4 contribution to CMIP6–Part 2: Two interglacials, scientific objective and experimental design for Holocene and Last Interglacial simulations, Geoscientific Model Development, 10, 3979-4003, 2017.

Park, E., Hefter, J., Fischer, G., Iversen, M. H., Ramondenc, S., Nöthig, E.-M., and Mollenhauer, G.: Seasonality of archaeal lipid flux and GDGT-based thermometry in sinking particles of high-latitude oceans: Fram Strait (79° N) and Antarctic Polar Front (50° S), Biogeosciences, 16, 2247-2268, 2019.

Parkinson, C. L., and Cavalieri, D. J.: Antarctic sea ice variability and trends, 1979-2010, The Cryosphere, 6, 871-880, 2012.

946 Parkinson, C. L.: A 40-y record reveals gradual Antarctic sea ice increases followed by
947 decreases at rates far exceeding the rates seen in the Arctic, Proceedings of the National
948 Academy of Sciences, 116, 14414-14423, 2019.
949 Paul, S., Willmes, S., and Heinemann, G.: Long-term coastal-polynya dynamics in the southern
950 Weddell Sea from MODIS thermal-infrared imagery, The Cryosphere, 9, 2027-2041, 2015.
951 Pritchard, H., Ligtenberg, S., Fricker, H., Vaughan, D., Van den Broeke, M., and Padman, L.:
952 Antarctic ice-sheet loss driven by basal melting of ice shelves, Nature, 484, 502-505, 2012.
953 Raddatz, T., Reick, C., Knorr, W., Kattge, J., Roeckner, E., Schnur, R., Schnitzler, K.-G.,
954 Wetzel, P., and Jungclaus, J.: Will the tropical land biosphere dominate the climate–carbon
955 cycle feedback during the twenty-first century?, Climate dynamics, 29, 565-574, 2007.
956 Riaux-Gobin, C., and Poulin, M.: Possible symbiosis of Berkeleya adeliensis Medlin,
957 Synedropsis fragilis (Manguin) Hasle et al. and Nitzschia lecointei Van Heurck
958 (Bacillariophyta) associated with land-fast ice in Adélie Land, Antarctica, Diatom Research,
959 19, 265-274, 2004.
960 Riaux-Gobin, C., Dieckmann, G. S., Poulin, M., Neveux, J., Labrune, C., and Vetion, G.:
961 Environmental conditions, particle flux and sympagic microalgal succession in spring before
962 the sea-ice break-up in Adélie Land, East Antarctica, Polar Research, 32,
963 https://doi.org/10.3402/polar.v32i0.19675, 2013.
964 Rintoul, S., Hughes, C., and Olbers, D.: The Antarctic circumpolar current system, International
965 Geophysics, 77, 271-302, 2001.
966 Roeckner, E., Dümenil, L., Kirk, E., Lunkeit, F., Ponater, M., Rockel, B., Sausen, R., and
967 Schlese, U.: The Hamburg version of the ECMWF model (ECHAM), Research activities in
968 atmospheric and oceanic modelling. CAS/JSC Working Group on Numerical
969 Experimentation, 13, 7.1-7.4, 1989.

970 Sangrà, P., Gordo, C., Hernández-Arencibia, M., Marrero-Díaz, A., Rodríguez-Santana, A.,
971 Stegner, A., Martínez-Marrero, A., Pelegrí, J. L., and Pichon, T.: The Bransfield current
972 system, Deep Sea Research Part I: Oceanographic Research Papers, 58, 390-402, 2011.
973 Scambos, T. A., Bell, R. E., Alley, R. B., Anandakrishnan, S., Bromwich, D., Brunt, K.,
974 Christianson, K., Creyts, T., Das, S., and DeConto, R.: How much, how fast?: A science
975 review and outlook for research on the instability of Antarctica's Thwaites Glacier in the
976 21st century, Global and Planetary Change, 153, 16-34, 2017.
977 Schmidt, K., Brown, T. A., Belt, S. T., Ireland, L. C., Taylor, K. W., Thorpe, S. E., Ward, P.,
978 and Atkinson, A.: Do pelagic grazers benefit from sea ice? Insights from the Antarctic sea
979 ice proxy $IPSO_{25}$, 15, 1987-2006, 2018.
980 Schmidtko, S., Heywood, K. J., Thompson, A. F., and Aoki, S.: Multidecadal warming of
981 Antarctic waters, Science, 346, 1227-1231, 2014.
982 Schofield, O., Brown, M., Kohut, J., Nardelli, S., Saba, G., Waite, N., and Ducklow, H.:
983 Changes in the upper ocean mixed layer and phytoplankton productivity along the West
984 Antarctic Peninsula, Philosophical Transactions of the Royal Society A: Mathematical,
985 Physical and Engineering Sciences, 376, https://doi.org/10.1098/rsta.2017.0173, 2018.
986 Schouten, S., Hopmans, E. C., Schefuß, E., and Sinninghe Damsté, J. S.: Distributional
987 variations in marine crenarchaeotal membrane lipids: a new tool for reconstructing ancient
988 sea water temperatures?, Earth and Planetary Science Letters, 204, 265-274, 2002.
989 Schouten, S., Hopmans, E. C., and Sinninghe Damsté, J. S.: The organic geochemistry of
990 glycerol dialkyl glycerol tetraether lipids: A review, Organic Geochemistry, 54, 19-61, 2013.
991 Schröder, M.: The Expedition PS111 of the Research POLARSTERN to the southern Weddell
992 Sea in 2018, Berichte zur Polar-und Meeresforschung = Reports on polar and marine
993 research, 718, 2018.
994 Sidorenko, D., Goessling, H., Koldunov, N., Scholz, P., Danilov, S., Barbi, D., Cabos, W.,
995 Gurses, O., Harig, S., and Hinrichs, C.: Evaluation of FESOM2. 0 coupled to ECHAM6. 3:

996 Preindustrial and HighResMIP simulations, Journal of Advances in Modeling Earth
997 Systems, 11, 3794-3815, 2019.
998 Smik, L., Belt, S. T., Lieser, J. L., Armand, L. K., and Leventer, A.: Distributions of highly
999 branched isoprenoid alkenes and other algal lipids in surface waters from East Antarctica:
1000 further insights for biomarker-based paleo sea-ice reconstruction, Organic Geochemistry,
1001 95, 71-80, 2016.
1002 Spencer-Jones, C. L., McClymont, E. L., Bale, N. J., Hopmans, E. C., Schouten, S., Müller, J.,
1003 Abrahamsen, E. P., Allen, C., Bickert, T., Hillenbrand, C. D., Mawbey, E., Peck, V.,
1004 Svalova, A., and Smith, J. A.: Archaeal Intact Polar Lipids in Polar Waters: A Comparison
1005 Between the Amundsen and Scotia Seas, Biogeosciences Discuss. [preprint],
1006 https://doi.org/10.5194/bg-2020-333, in review, 2020.
1007 Stevens, B., Giorgetta, M., Esch, M., Mauritsen, T., Crueger, T., Rast, S., Salzmann, M.,
1008 Schmidt, H., Bader, J., and Block, K.: Atmospheric component of the MPI-M Earth system
1009 model: ECHAM6, Journal of Advances in Modeling Earth Systems, 5, 146-172, 2013.
1010 Stocker, T. F., Qin, D., Plattner, G.-K., Tignor, M., Allen, S. K., Boschung, J., Nauels, A., Xia,
1011 Y., Bex, V., and Midgley, P. M.: The physical science basis. Contribution of working group
1012 I to the fifth assessment report of the intergovernmental panel on climate change,
1013 Computational Geometry, 18, 95-123, 2013.
1014 Tesi, T., Belt, S., Gariboldi, K., Muschitiello, F., Smik, L., Finocchiaro, F., Giglio, F., Colizza,
1015 E., Gazzurra, G., and Giordano, P.: Resolving sea ice dynamics in the north-western Ross
1016 Sea during the last 2.6 ka: From seasonal to millennial timescales, Quaternary Science
1017 Reviews, 237, http://dx.doi.org/10.1016/j.quascirev.2020.106299, 2020.
1018 Thomas, D. N.: Sea ice, John Wiley & Sons, 2017.
1019 Thompson, A. F., Heywood, K. J., Thorpe, S. E., Renner, A. H., and Trasviña, A.: Surface
1020 circulation at the tip of the Antarctic Peninsula from drifters, Journal of Physical
1021 Oceanography, 39, 3-26, 2009.

1022 Thompson, A. F., Stewart, A. L., Spence, P., and Heywood, K. J.: The Antarctic Slope Current
1023 in a changing climate, Reviews of Geophysics, 56, 741-770, 2018.
1024 Turner, J., Orr, A., Gudmundsson, G. H., Jenkins, A., Bingham, R. G., Hillenbrand, C.-D., and
1025 Bracegirdle, T. J.: Atmosphere-ocean-ice interactions in the Amundsen Sea Embayment,
1026 West Antarctica, Reviews of Geophysics, 55, 235-276, 2017.
1027 Valcke, S.: The OASIS3 coupler: A European climate modelling community software,
1028 Geoscientific Model Development, 6, 373-388, 2013.
1029 Vaughan, D. G., Marshall, G. J., Connolley, W. M., Parkinson, C., Mulvaney, R., Hodgson, D.
1030 A., King, J. C., Pudsey, C. J., and Turner, J.: Recent rapid regional climate warming on the
1031 Antarctic Peninsula, Climatic change, 60, 243-274, 2003.
1032 Vaughan, D. G.: West Antarctic Ice Sheet collapse–the fall and rise of a paradigm, Climatic
1033 Change, 91, 65-79, 2008.
1034 Vernet, M., Geibert, W., Hoppema, M., Brown, P. J., Haas, C., Hellmer, H., Jokat, W., Jullion,
1035 L., Mazloff, M., and Bakker, D.: The Weddell Gyre, Southern Ocean: present knowledge
1036 and future challenges, Reviews of Geophysics, 57, 623-708, 2019.
1037 Volkman, J. K.: Lipid markers for marine organic matter, in: Marine organic matter:
1038 Biomarkers, isotopes and DNA, Springer, 27-70, 2006.
1039 Vorrath, M.-E., Müller, J., Esper, O., Mollenhauer, G., Haas, C., Schefuß, E., and Fahl, K.:
1040 Highly branched isoprenoids for Southern Ocean sea ice reconstructions: a pilot study from
1041 the Western Antarctic Peninsula, Biogeosciences, 16, 2961-2981, 2019.
1042 Vorrath, M.-E., Müller, J., Rebolledo, L., Cárdenas, P., Shi, X., Esper, O., Opel, T., Geibert,
1043 W., Muñoz, P., and Haas, C.: Sea ice dynamics in the Bransfield Strait, Antarctic Peninsula,
1044 during the past 240 years: a multi-proxy intercomparison study, Climate of the Past, 16,
1045 2459-2483, 2020.

1046 Xiao, X., Fahl, K., Müller, J., and Stein, R.: Sea-ice distribution in the modern Arctic Ocean:
1047 Biomarker records from trans-Arctic Ocean surface sediments, Geochimica et
1048 Cosmochimica Acta, 155, 16-29, 2015.
1049 Zamelczyk, K., Rasmussen, T. L., Husum, K., Haflidason, H., de Vernal, A., Ravna, E. K.,
1050 Hald, M., and Hillaire-Marcel, C.: Paleoceanographic changes and calcium carbonate
1051 dissolution in the central Fram Strait during the last 20 ka, Quaternary Research, 78, 405-
1052 416, 2012.
1053 Zielinski, U., Gersonde, R., Sieger, R., and Fütterer, D.: Quaternary surface water temperature
1054 estimations: Calibration of a diatom transfer function for the Southern Ocean,
1055 Paleoceanography and Paleoclimatology, 13, 365-383, 1998.
1056 Zwally, H. J.: Antarctic sea ice, 1973-1976: Satellite passive-microwave observations,
1057 Scientific and Technical Information Branch, National Aeronautics and Space, 1983.